# The first steps toward the creation of a bioink for endochondral bone regeneration

A thesis by Anne Kuijper

Department of Oral and Maxillofacial Surgery, Prosthodontics and Special Dental Care

Supervised by Debby Gawlitta & Leanne de Silva

November, 2023

# Abstract

The treatment of critical-sized bone defects poses significant challenges as these defects often require medical intervention. The gold standard treatment, autologous bone grafts, has drawbacks like donor site morbidity and limited tissue availability. In response, the field of bone tissue engineering (BTE) emerged, aiming to develop biological substitutes or scaffolds utilizing biomaterials, cells, and growth factors to regenerate bone. However, challenges such as insufficient vascularization still hinder clinical translation. Nonetheless, endochondral bone regeneration (EBR) is a BTE approach that holds promise. It involves mimicking a soft callus to serve as template for bone regeneration.

This thesis focuses on advancing the EBR research of our group by developing a bioink containing chondrogenic micro pellets. A microwell system was selected to generate micro pellets, which were cultured across four mesenchymal stem cell donors. Seven different cell densities (1500, 3000, 6000, 12000, 24000, 36000, and 50,000 cells per micro pellet) and a control (250,000 cells per macro pellet) were analyzed for size and chondrogenic differentiation with a safranin-O, toluidine blue, and collagen II staining. In continuation, micro pellets were combined with Gelatin Methacryloyl (GelMA) to create a bioink, which was cast and volumetrically printed to demonstrate functionality by fabricating an incus bone shape.

The microwell system of the Inge Zuhorn group was chosen for further optimization instead of microwell stamps. Micro pellets under 6000 cells displayed limited to no GAG and collagen II deposition. Above 6000 cells, micro pellets demonstrated unwanted aggregation but exhibited complete GAG and collagen II deposition. Due to these issues, a second bioink, composed of crushed macro pellets and GelMA, was formulated. The macro pellets were effectively crushed and integrated into bioink and used to volumetrically print an incus bone.

In conclusion, a microwell system was selected, the initial steps to optimize micro pellet culture were taken, and a successful bioink for EBR was formulated and printed. Optimizing and standardizing chondrogenic micro pellet culture, bioink formulation, and printing through further experimentation is recommended for future applications.

# Layman's summary

Large injuries in bone cannot heal by themselves and require medical intervention. Standardly these injuries are treated by taking bone from another part of the body and placing it at the site of injury. However, this comes with disadvantages such as a limited supply and a new injury at the site where bone was taken. Sometimes bone from another patient is taken and used as an alternative. Yet this has limitations as well, such as risk of disease transmission and rejection by the recipient's immune system. Regenerative medicine is a research field that focusses on finding materials, cells, or specific proteins that support and guide the body to heal injuries, such as large bone defects.

Bone can be formed in two ways and of them is called endochondral ossification (ECO). During this complicated process, soft cartilage is laid down as a framework so the body can gradually transform it into hard bone. In this thesis, the goal was to mimic that cartilage framework in different sized little balls, called micro pellets, and combine them with a hydrogel, a polymer network that traps water. Together, they are called a bioink, which often consist of a hydrogel combined with all kinds of helpful cells, proteins, and molecules. A bioink is a special ink used in 3D bioprinters to fabricate pieces of tissue or organs. In addition to the first bioink, the goal was to make a second bioink with bigger versions of the micro pellets, called macro pellets, and the hydrogel. The macro pellets were crushed to a powder before they were combined with the hydrogel. After creating the bioinks, the goal was to use the bioinks to print the shape of an incus bone. The incus bone is one of the small ossicles in the ear and could be printed in its entirety. It has complex shape, which would be difficult to make with biological materials without the aid of 3D printing.

To create the cartilage-like micro and macro pellets, mesenchymal stem cells (MSCs) were used. MSCs are stem cells that can turn into fat, bone, and cartilage. To turn the stem cells to cartilage, specific growth factors are used. To get different sizes, different amounts of MSCs were used when growing the micro pellets. After 28 days, the micro and macro pellets were collected, their size evaluated, and assessed to see if they successfully turned into cartilage-like tissue.

We report that micro pellets that were made with a higher amount go MSCs clumped together when grown, which was something we did not want. In contrast, the micro pellets that were made with a lower amount of MSCs were not able to turn into the cartilage-like tissue. The micro pellets that did not clump together, and still showed some signs of being cartilage-like were chosen for the bioink. The macro pellets were successfully turned and grown into cartilage-like tissue and crushed into tiny pieces. Due to some complications, the first bioink with micro pellets was not tested with the 3D printer. Luckily, the bioink with crushed macro pellets was tested and could be effectively printed into the shape of an incus bone.

In conclusion, we showed that it was possible to 3D print a complex shape with bioink that is made from a hydrogel and crushed cartilage-like macro pellets. Moreover, we also demonstrated that we could grow different sized cartilage-like micro pellets. In the future, we will continue to optimize the growth of the micro pellets and the printing of the bioinks.

# Table of Contents

# General Introduction

## Challenges in the treatment of critical-sized bone defects

Bone is a dynamic tissue that undergoes constant remodeling throughout our lifetime and has great regenerative capacity (1,2). However, when bone is damaged, depending on the size of the defect and the circumstances surrounding the patient, not all bone defects will heal naturally (3). In such instances, medical intervention is required to restore bone in the defect site. The current golden standard for treatment of such critical-sized bone defects is an autologous bone graft (i.e., bone removed from one part of the patient's body and implanted in another site). However, since these grafts are sourced from the patient's own body, they are often accompanied by drawbacks such as donor site morbidity, limited tissue availability and long surgery times associated with graft retrieval and implantation (4,5). Alternatively, the use of allogenic bone grafts (i.e., bone donated from a different individual to the patient) circumvents these drawbacks. Nevertheless, allograft tissue has its own set of shortcomings, such as the risk of disease transmission and rejection of the graft by the hosts immune system (4). Thus, as the treatment of critical-sized bone defects can still be improved, alternative approaches in the field of regenerative medicine (RM) and bone tissue engineering (BTE) have been explored over the years.

## Regenerative medicine & bone tissue engineering

RM and BTE are multidisciplinary fields that involve the development of biological substitutes or scaffolds to repair or regenerate damaged or lost bone tissue. It includes mimicking and supporting the inherent capacity of bone to undergo self-repair and regenerate. The research fields focus on both acquired (e.g., trauma, tumor resection) and congenital (e.g., polyostotic fibrous dysplasia, osteogenesis imperfecta) bone injuries. RM includes different kinds of scaffolds using various biomaterials, cells, growth factors, and combinations thereof which have been implemented with the aim to replace the autograft bone (3). While the field has advanced, clinical translation remains difficult due to several challenges, such as insufficient vascularization, the laboriousness of cell-seeding techniques which must be 'good manufacturing practice' (GMP) produced, and the safety of administrating exogenous growth factors for a longer period of time (6)(7). An in-depth discussion of these approaches is beyond the scope of this thesis. Readers who are interested in a more in-depth discussion of the various approaches to bone tissue engineering are invited to read a fundamental review discussing the advances in the field written by Manzini et al (3).

## Bone repair

Cell-based techniques for bone repair involve the use of patient derived stem cells to drive the regeneration of bone. There are two main pathways of bone formation, endochondral ossification and intermembranous ossification (3). Earlier tissue engineering approaches aimed to mimic the intramembranous route by the direct differentiation of mesenchymal stem cells (MSCs) to osteoblasts, which can directly deposit bone matrix in the body. However, the lack of a functional vascular system has limited the translation of this approach to more clinically relevant construct sizes (7,8). Conversely, in bone repair, endochondral ossification relies on the differentiation of MSCs toward the chondrogenic lineage and the development of an intermediate soft callus. Endochondral bone regeneration (EBR) mimics this process and when implanted the transient avascular cartilage template containing bioactive molecules leads to the invasion of a vascular network and remodeling by osteoclasts. During the remodeling process, the cartilage template is gradually broken down and

osteoblasts become active which deposit calcified matrix on the cartilage remnants. Over time, the calcified matrix hardens, and this process eventually leads to the formation of new bone (9,10).

## Off-the-shelf chondrogenic devitalized spheroids

Our research group has been dedicated towards using EBR as a strategy for bone tissue engineering. In this approach, a cartilage mimetic is generated in the lab by differentiating allogeneic bone marrow derived MSCs encapsulated within a collagen hydrogel. After 28 days, the spheroids are devitalized (i.e., cells are killed) encapsulated within a hydrogel (e.g., fibrin or collagen) and implanted into a bone defect (11,12). The feasibility of our approach has been shown to induce bone formation in both a small and large animal model (11,13). Both papers show the feasibility of using off-the-shelf devitalized chondrogenic spheroids, derived from allogeneic MSCs, for bone regeneration.

## Volumetric bioprinting

In combination with a cell-based approach for bone repair, additive manufacturing, also known as 3D printing, can be used to make complex and personalized constructs. Critical-sized bone defects are often complex in shape. Using an additive manufacturing technique, patient-specific constructs with embedded biological components could be fabricated.

Volumetric bioprinting (VBP) is a specific bioprinting technique that can make complex structures within seconds to minutes instead of hours, which is a common drawback of other additive manufacturing techniques (14). Additionally, constructs printed with VBP are layerless and do not rely on support structures, which allows for freeform fabrication. This is made possible due to the way the ink is polymerized. In brief, filtered back projections of the desired construct are beamed onto a revolving container containing the photocrosslinkable bioink with visible light. The total energy of the visible light surpasses the crosslinking threshold of the bioink in the specific locations where the desired construct was projected, which results in the polymerization of bioink and the creation of the construct (15,16).

A bioink for VBP can incorporate cells or tissue constructs like organoids. However, a drawback arises because VBP is most effective with bioinks that have a high optical transparency. Particles inside of the ink will scatter the light and cause irregularities. Bigger particles will cause more light scattering and can cast a shadow, which lowers the resolution of the printed construct (14). However, there is a complex new technique that is able to correct for the scattering as described in the paper by Madrid-Wolff et al. (17). In addition to this technique, which corrects scattering before computing the projecting patterns for the constructs, iodixanol can also be used. Iodixanol is a substance which makes the light refraction index of particles inside the bioink identical to hydrogel bulk of the bioink (16).

## Micro pellets as bioink

Micro pellets are smaller versions of the ‘macro’ pellet or spheroid containing 1 to 5 x $10^5$ cells and are biomaterial-free. Micro pellets, often termed micro tissues, can be useful as building blocks for bigger or more complex tissues and can be made in a high throughput manner (18–20).

As micro pellets are much smaller than macro pellets, they might be more ideal for VBP bioink. They cast a smaller shadow, which could be easier to correct for. The same might be the case for the scattering of the light. Moreover, micro pellets are pipette-able, thus a micro pellet based bioink could be used for extrusion based bioprinters as well.

Continuing and combining the research of our group, the micro pellets can be devitalized before being incorporated in a bioink. An advantage of using devitalized micro pellets in printed constructs; there are no living cells present in the bioink that require specific conditions. Furthermore, the presence of free radicals generated during the photo-polymerization process will not harm the cells. It is also theorized that post-printing, batches of unpolymerized bioink could be reused due to the devitalized nature of the pellets. A scenario which is currently impractical with living cells, as there may be loss of cellular functionality. Ultimately, the absence of viable cells in the devitalized micro pellets may extend their storage stability and shelf life.

## Outline and aim

The main aim of this thesis was to create a bioink for EBR.

To achieve this goal, three main sub aims were addressed:

1. To establish a microwell system for the generation of micro pellets.
2. To generate micro pellets in a range of sizes and study the effect of donor age and cell number per micro pellet on the chondrogenic differentiation potential.
3. To demonstrate the initial proof of concept regarding the formulation of a bioink and the printability with a volumetric bioprinter.

This thesis will be divided into three sections, each corresponding to a sub-aim. To begin, the first section will delve into the initial sub-aim, and so on.

# Part 1 – Microwell systems

# Methods

## Study design

To generate micro pellets, it was necessary to establish a platform for their culture (Figure 1). The goal was to create agarose microwells, as agarose was freely available within the laboratory and previous testing had been done with the material. To create the microwell indentations in agarose, a microwell stamp was printed with a digital light processing (DLP) printer.

Two different types of stamps were DLP printed: one with cone-shaped microwell protrusions and another with U-shaped microwell protrusions. Every microwell stamp featured 123 individual cone- or U-shaped microwell protrusions. Each microwell protrusion had a dimension of 1 mm in diameter and 1 mm in height. The shape of the microwell protrusions and the ability of the stamps in producing microwells within an agarose gel was evaluated with an Olympus SZ61 stereomicroscope and Olympus IX53 microscope respectively. The stamps were compared to their original Autodesk Fusion 360 model in terms of size, to ensure accuracy and precision.

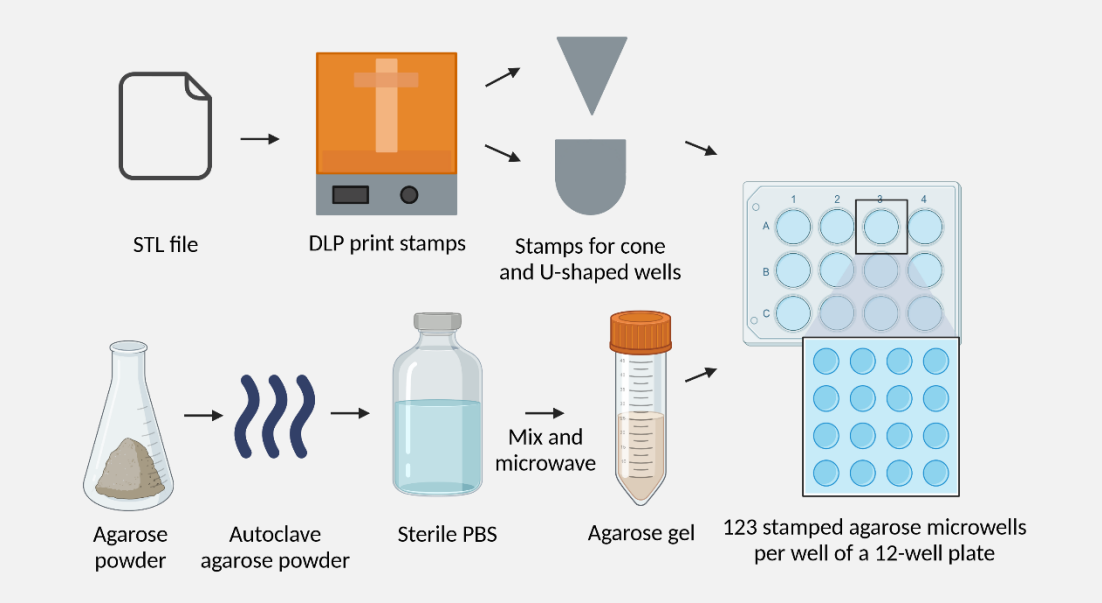


*Figure 1. Overview of the design, creation, and fabrication of agarose microwells.*

## Creation of the microwell system

An STL file was generated by modeling the microwell stamps in Autodesk Fusion 360 software (Figure 2). The microwell stamps were DLP printed (EnvisionTEC) with PIC-100 resin (EnvisionTEC). After printing, postprocessing involved two washing steps with ethanol in a sonicator bath. Thereafter, the parts were post-cured in an ultraviolet (UV)-oven with 3000 flashes of UV light as instructed in protocol 3 (page 5 of 'Laboratory Protocols').

To produce the microwells with the printed stamps, molecular biology grade agarose powder (28040L, Eurogentec) and sterile PBS0 were mixed in a 2 % w/v concentration by following protocol 4 (page 6 of 'Laboratory Protocols'). The solution was heated in a microwave until the solution was clear, liquid,

and no bubbles remained. As agarose undergoes thermal gelation, the agarose solution was maintained in a water bath or oven at 90 °C to keep it in a liquid state until further use. In cases where sterility was essential, the agarose powder was autoclaved before being mixed.

The microwell stamps were designed to be compatible with a 12-well plate. Each well was filled with 2.5 ml of agarose solution, and the stamps were promptly placed on top. The agarose gel was left to solidify for 5 minutes, after which the microwell stamps could be removed. To ensure that no residual agarose was left in the wells, the plates were washed with PBS and then centrifuged for 8 minutes at 900 rpm (21). Subsequently, the PBS was aspirated. The integrity of the microwells was confirmed by inspecting them under an Olympus SZ61 stereomicroscope.

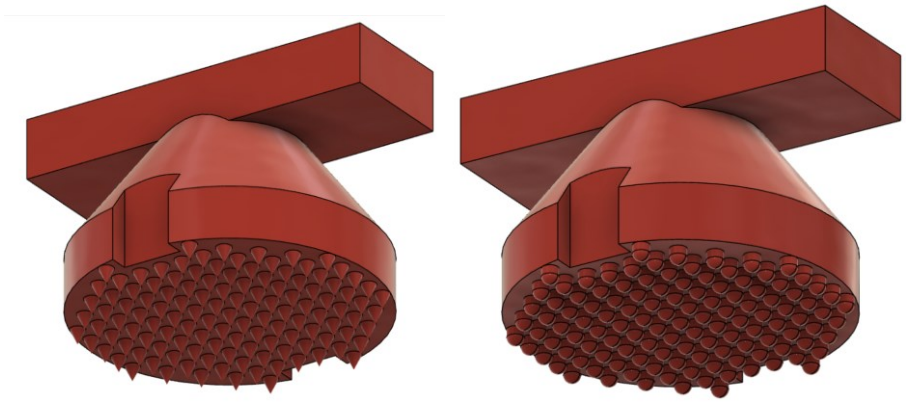

*Figure 2. Models of the two microwell stamps. On the left, the cone-shaped microwell stamp and on the right the U-shaped microwell stamp. Both the cone and U-well shaped microwell were 1 mm in diameter and height.*

## Assessment of the microwell stamps

The microwell stamps were assessed in terms of protrusion shape and function. The shape of the microwell stamps was evaluated under the Olympus SZ61 stereomicroscope. The diameter of the cone and U-well shaped protrusions was measured with ImageJ v1.54d. software and compared to the original Autodesk fusion 360 model. For each microwell stamp, six measurements were conducted, three at random in the periphery and three at random in the center. Subsequently, the averages and standard deviation (SD) were calculated.

The performance of the stamps was assessed by producing agarose microwells. The agarose solution was prepared and stamped, whereafter the indentations were evaluated for imperfections under the Olympus IX53 microscope. Imperfections encompassed variations in diameter and shape among microwells.

## Statistics

A one-way ANOVA with subsequent Tukey post hoc testing was conducted on the measurements of the diameters of both U-shaped and cone-shaped microwell protrusions of the microwell stamps. The multiple comparisons analysis within the one-way ANOVA aimed to compare the average measurements of the periphery and the center, as well as to compare both the center and the periphery measurements to the original size in the STL file.

# Results

To evaluate the quality of the DLP printed stamps, they were examined under a microscope. The total overview of the seven cone and five U-well shaped microwell stamps can be found in Appendix 1 and Appendix 2 respectively.

The resolution of the DLP printer affected the space between individual printed microwell protrusions on the bottom of the stamps, which resulted in fusion of the U-well protrusions. In Figure 3C side view, the fusion of these protrusions is visible. In Figure 3D, attempts were made to eliminate the residual resin between the protrusions by washing with 100% ethanol, however in both the bottom and side view, an excess of grainy resin appeared to persist. Visually, the cone shaped microwell stamps showed discrepancies between the periphery and the center of the stamp. In Figure 3A and B, the apex of several cone shaped microwell protrusions were missing.

The measured average diameter of the cone-shaped microwell protrusions in the periphery of the stamp is larger than in the original STL file. Furthermore, both in the periphery and at the center, the microwell protrusions of the U-well stamp are larger than those in the original STL file. However, there was no difference in diameter between the periphery and center microwell protrusions for both cone and U-well-shaped microwell stamps (Figure 4).

The discrepancies between the printed microwell stamps and the original STL files are reflected in the agarose microwells that were made (Figure 5). For the cone-shaped microwells, the white arrows indicate the variation in microwell diameter achieved with a single stamp. For the U-wells, the white arrows illustrate the impact of the fusion of the U-wells on a stamp, resulting in low discernibility of individual agarose microwells.

A summary of the errors among the respective microwell stamps is visualized in Table 1. The defects were predominantly located in the center of the microwell stamps.

| | **Cone (N = 7)** |
|---|---|
| *Missing apex* | 5 |
| *Discrepancy in diameters* | 5 |

| | **U-well (N = 5)** |
|---|---|
| *Grainy resin residue* | 4 |
| *Fusion of microwells* | 1 |

*Table 1. An overview of both the quantity and category of microwell stamps with defects, as well as the specific type of defect. Notably, a single stamp can manifest multiple defect types.*

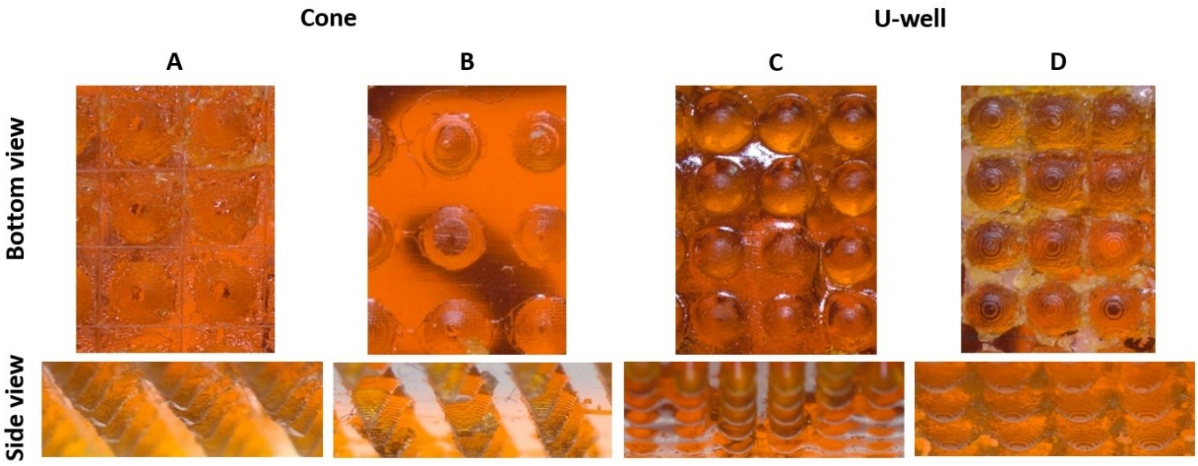


*Figure 3. Four microwell stamps that represent the total batch of DLP printed microwells illustrated in Appendix 2 and 3. These figures were magnified versions of the figures in Appendix 2 and 3 to highlight the errors in the individual microwell stamps.*

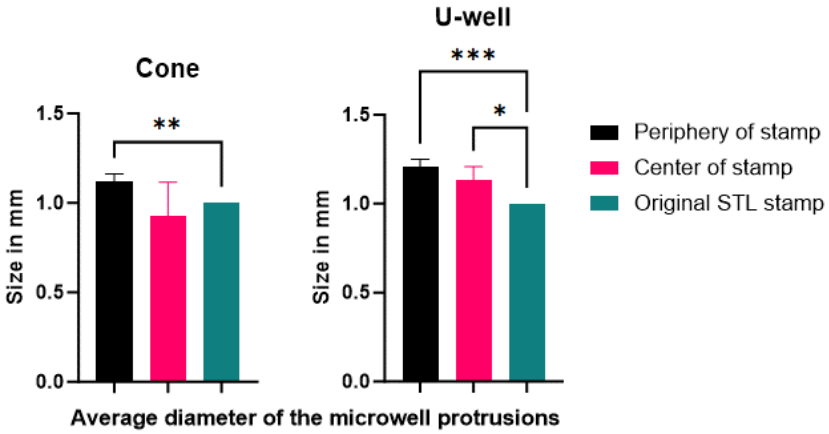


*Figure 4. Average diameter of the microwells protrusions at the bottom of the stamp in mm. A multiple comparisons test between average diameters is shown. * 0.05, ** 0.01, *** 0.001, **** <0.0001.*

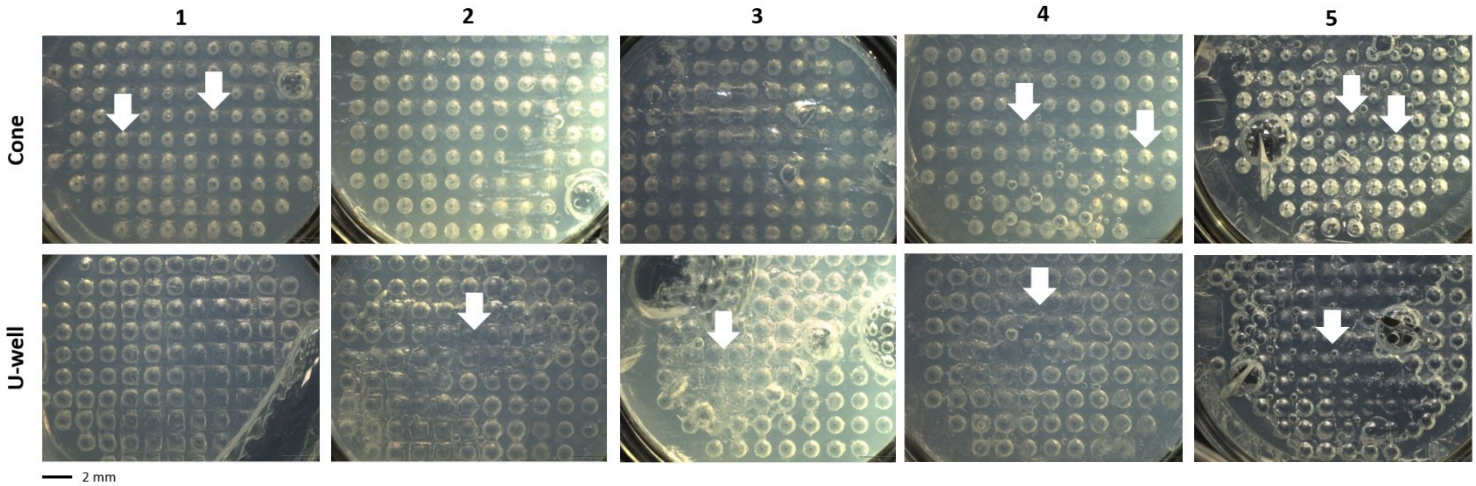


*Figure 5. Agarose microwells. The white arrows in the top row show the variation in microwell diameters. The white arrows in the bottom row show the effect of the fusion of the U-wells. The microscopic images include a scalebar measuring 2 mm.*

# Discussion and conclusions

The design of the microwell stamps was based on previous designs in the laboratory and on the microwell stamp made by Gonzalez-Fernandez et al. (21). In contrast to the results of Gonzalez-Fernandez et al. (21), the microwell stamps of this experiment were printed with varying degrees of success.

During the design process, the resolution of the DLP printer was taken into account. Experts in our laboratory knew from experience that the practical resolution did not reach the ideal 25 µm. Consequently, the dimensions of the microwell protrusions were kept relatively large. Print resolution is affected by various factors, such as print size, layer height, and Z-axis stability. Additionally, post-processing steps, such as post-curing and ethanol washing, can impact the printed structures as well (22). For future experiments involving DLP printing, it is advisable to fine-tune the printer settings to improve the resolution.

In the results, a trend visible was the fusion of the U-well shaped protrusions of the stamps. In contrast, little fusion of the cone-shaped microwells protrusions took place. The U-shaped microwells fused along the vertical wall of the U-shape, and while it can be argued that the half-moon shape at the bottom is the most important part of the microwell, the vertical walls were hypothesized to lessen the chance of crosstalk between separate wells. The U-wells could be spaced further apart to obtain a better stamp resolution. In addition, the orientation of the stamp while printing could also influence the resolution. If the stamps were printed on an angle with supports, the resolution could potentially be improved as well (22,23).

Overall, the cone-shaped microwells possessed preferable functionality in contrast to the U-shaped microwells. The fusion of the U-shaped microwells rendered the agarose microwells nonfunctional. The U-shape was picked because the spheroids from Longoni et al. (11,12) research were cultured in 96-well plates, which also have a concave shape. The cone shape was picked to compare to the U-shaped microwells as it has been hypothesized in our group that the cone-shape might cause inhomogeneous matrix deposition. The tapered end of the cone might cause the oxygen tension and nutrient availability to be different at the sides and bottom of the micro pellet, in comparison to the top, due to differences in diffusion distance.

Guo et al. (24) suggests that the U-shape is the preferred microwell shape for micro pellet culture in comparison to cuboid or cylindrical shaped microwells. Nevertheless, Thomsen et al. (25) developed a cone shaped microwell system, which facilitated 3D cell culture, promoted cellular self-organization, and therefore cell aggregate formation. Consequently, a conical shape might serve as an effective approach for micro pellet creation as well. Moreover, Selimović et al. (26) contend that U-shaped and conical microwells provide enhanced media circulation compared to cylindrical microwells. Thus, focusing on conical microwells alone could be equally efficient as U-shaped microwells for micro pellet culture.

However, on both types of stamps the individual microwell protrusions exhibited variations in diameter. These differences may have implications for the dimensions of the resulting micro pellets. Consistency in micro pellet size is crucial for ensuring the reproducibility of the experiment. This consistency is unattainable if the microwells inherently possess irregularities. Due to the irreproducibility of the DLP printed microwell stamps, a collaboration was made with the Biomedical Engineering department of Groningen University, group of Inge Zuhorn, with PhD student Alejandro Reina Mahecha.

Zuhorn's research group has developed a microwell system that is both established and innovative. The microwell system was composed of PDMS, with a single PDMS well fitting into the well of a 6-well plate. Each well contained 12 macro wells, which all included 19 microwells. As a result, a single well can accommodate up to 228 microwells (Figure 6). One of the key advantages of this microwell system is that the PDMS molds can be reused after autoclaving. Additionally, the molds can be customized regarding the quantity of macro wells and microwells, which is beneficial for fine-tuning the hMSC number per well, and for enhancing the scalability and streamlined collection of micro pellets. Because the microwell system has already been established, it would require little optimization in terms of microwell system production and reproducibility.

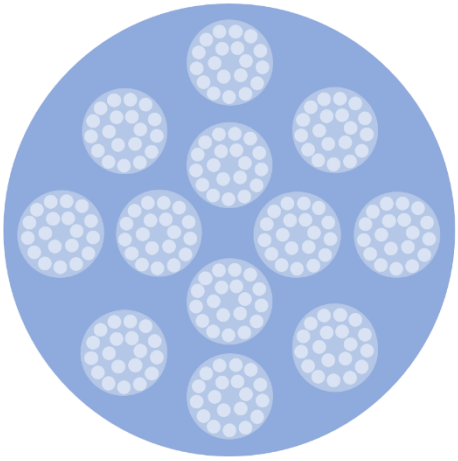

*Figure 6. 2D image depicting the layout of the PDMS wells made by the group of Inge Zuhorn. The large circle is referred to as the well, the 12 middle-sized circles as macro wells, and the 228 smallest circles as microwells.*

## Conclusion

In conclusion, although the production of agarose microwells using the DLP-printed microwell stamps was achievable, the process required further optimization to ensure the reliability and reproducibility of the fabricated microwells. As a result, the decision was made to adopt the optimized microwell system developed by Inge Zuhorn's group at Groningen University.

# Part 2 – Micro pellets

# Methods

## Study design

Micro pellets were cultured using human bone marrow-derived MSCs (BM-MSCs) from four distinct donors (referred to as donor A, B, C, and D, corresponding to donor 52, 53, 56, and 59, respectively). A range of different seeding densities was assessed in the microwells (Table 2). An additional experimental group was taken along in a 96-well plate and consisted of 50,000 cells per well. A control group, referred to as group 8 and composed of 250,000 cells per well, was cultured in a 96-well plate as well. All the groups were cultured for 28 days (Figure 7). The chondrogenic differentiation was analyzed by histology and the pellet diameter with light microscopy. The light microscopes Olympus BX43 and Olympus IX53 were used respectively.

In a pilot study, donor C was used to determine if hMSCs formed micro pellets in the PDMS microwells and if the range of the cell seeding density was feasible (Table 2). Additionally, the pilot study was used to determine the best method of pellet collection and to assess if micro pellets differentiated in the same timely manner as macro pellets. Donor C, group 1 and 6, were harvested on day 7, 14, 22, and 28-30 (based on whether the final collection day was during a weekday). The remaining groups were harvested on day 28-30 as well. Group 7 was not included in the pilot study.

Two of the donors, A and C, are defined as old (age > 70) and the other two donors, B and D, as young (age < 20 years). The cells of donor A were isolated at age 74 and the cells of donor C at age 71. The cells of donors B and D were both isolated at age 19.

| **Group 1 (cells/well)** | **Group 2 (cells/well)** | **Group 3 (cells/well)** | **Group 4 (cells/well)** | **Group 5 (cells/well)** | **Group 6 (cells/well)** | **Group 7 (cells/well)** | **Control/group 8 (cells/well)** |
|---|---|---|---|---|---|---|---|
| **1500** | 3000 | 6000 | 12000 | 24000 | 36000 | 50,000 | 250,000 |

*Table 2. Overview of the number of cells per well for the experimental groups and control that were used to form micro pellets.*

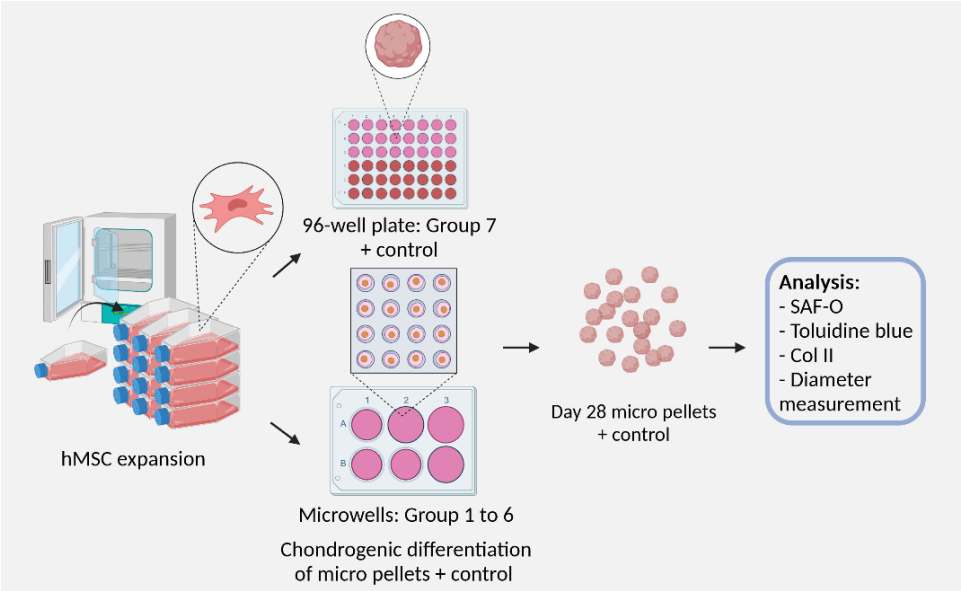


*Figure 7. Overview of the chondrogenic culture, collection, and analysis of experimental micro pellet groups and the control.*

## Expansion of human BM-MSC

Human BM-MSCs from four different donors (donor A, B, C, and D) were thawed and subsequently expanded in T175 flasks according to protocol 2 (page 3 of 'Laboratory Protocols'). The cells were cultured in MSC expansion medium which consists of α-MEM with 2 mM l-glutamine (22561, Gibco), 10 % heat-inactivated fetal bovine serum (FBS) (S14068S1810, Biowest), 0.2 mM L-ascorbic acid-2-phosphate (A8960, Sigma-Aldrich), 100 U/mL penicillin with 100 mg/mL streptomycin (15140, Gibco), and basic fibroblast growth factor (bFGF) (233-FB, R&D Systems). Due to the short shelf life of bFGF, it was added fresh at a concentration of 1 ng/ml. The medium was changed one day after plating and subsequently replaced three times a week.

The flasks were maintained in an incubator at 37 °C, with 5% carbon dioxide, and under humidified conditions. At a confluency of 80% the cells were passaged with trypsin and replated. Upon reaching passage 4, the cells were ready for use, and any surplus cells were cryopreserved for future application.

## Micro pellet formation and collection

**Formation of the macro and micro pellets**

The micro pellets were formed with passage 4 human BM-MSCs in PDMS microwells. The Inge Zuhorn group in Groningen made and tested the PDMS wells. To ensure sterility, the PDMS microwells were autoclaved before usage.

The micro pellets were cultured in chondrogenic differentiation medium consisting of DMEM containing glutamax and pyruvate (31966, Gibco), 1% ITS+ premix (354352, Corning), 0.1 µM Dexamethasone (D8893, Sigma-Aldrich), 0.2 mM L-ascorbic acid-2-phosphate, 100 U/mL penicillin with 100 mg/mL streptomycin (15140, Gibco), and growth factors BMP-2 (InductOS, Wyeth/Pfizer) and TGF-β1 (100-21, Pepro-tech). The growth factors were added fresh at a concentration of 100 ng/mL and 10 ng/ml respectively, according to protocol 1 (page 2 of 'Laboratory Protocols). The medium was changed three times a week and the first three days after plating.

Before use, according to protocol 5 (page 7 of 'Laboratory Protocols'), the sterile PDMS microwells were pre-conditioned at room temperature by adding 100 µl chondrogenic differentiation media, without growth factors, to the macro-wells, followed by centrifugation at 400*g* for 1 minute. Thereafter, the cells could be added to the macro-wells in a suspension of 100 µl chondrogenic medium and were centrifuged at 400*g* for 4 minutes. The plates were placed in the incubator for 24 hours to assess micro pellet formation. Following incubation, 2 ml of chondrogenic media was applied to cover the macro-wells in each well. In the case where micro pellets had not yet formed, protocol 5 would have been repeated.

The control macro pellets in the 96-well plate were formed following protocol 5 (page 7 of 'Laboratory Protocols). In the wells of the 96-well plate, a 200 µl suspension of chondrogenic medium containing cells was introduced. Subsequently, the plate was centrifuged at 300*g* for 5 minutes to promote pellet formation.

The cultures for all groups were maintained for 28 days and harvested between day 28 and 31. The plates with cells were kept in an incubator at 37 °C, with 5% carbon dioxide, under humidified conditions.

**Collection of the macro and micro pellets**

Micro pellets were collected by removing the 2 ml media on top of the well and flushing each macro-well separately with the media still present as stated in protocol 5 (page 7 of 'Laboratory Protocols). The plates were tilted 60°, this encouraged the flushed-out micro pellets to gather at the bottom of each macro-well. To generate enough force to flush the pellets out, a P200 pipet was used. The micro pellets were gathered in a 2 ml Eppendorf tube with a P1000 pipet to avoid damaging the pellets. In the case aggregates of pellets were present, a small spoon was used to collect the aggregates.

Each group (N= approx. 228) was gathered and divided into two Eppendorf tubes, one for histological examination and one for the diameter measurements. The micro pellets in the tubes were washed with PBS twice, whereafter the bulk of PBS was removed with a P1000 pipet. Subsequently, to preserve the micro pellets, approximately 1.5 to 2 ml of 4% formaldehyde was added. To maximize the dilution of PBS without risking the loss of micro pellets, the residue of PBS was diluted with 4% formaldehyde twice. The control pellets were collected with a small spoon and deposited in a 2 ml Eppendorf tube. Afterward, the pellets were washed and stored in the same manner as the micro pellets.

## Assessment of micro pellet diameter

To evaluate the size of the micro pellets, the pellets were transferred from the Eppendorf tubes to a petri dish. A few drops of 4% formaldehyde containing micro pellets were extracted after resuspension using a P1000 pipette and spread on a petri dish. Subsequently, the micro pellets were imaged under an Olympus IX53 microscope or Olympus SZ61 stereomicroscope. The diameter of the pellets was measured with Olympus cellSens Entry 4.1.1 imaging software, which was directly connected to the microscopes. A built-in measurement tool was used to draw a line along the diameter of each individual micro pellet. The program automatically measured the length of the line based on the applied magnification. The corresponding size was written down in Microsoft Excell 365.

In Microsoft Excel 365, the average and SD of each group was calculated. In Table 3, the number of micro pellets that were measured per group, per donor is specified. The variations in the numbers were due to the inability to handle a micro pellet individually. The diameter of each micro pellet on the petri dish was determined. Given the small volume used during pipetting, the number of micro pellets per petri dish differs between groups.

| Group (cell/well) | 1 (15000) | 2 (3000) | 3 (6000) | 4 (12000) | 5 (24000) | 6 (36000) | 7 (50,000) | 8 - control (250,000) |
|---|---|---|---|---|---|---|---|---|
| *Donor A (N)* | 40 | 16 | 46 | 45 | 10 | 8 | 3 | 6 |
| *Donor B (N)* | 11 | 11 | 12 | 22 | 14 | 12 | 4 | 5 |
| *Donor D (N)* | 19 | 14 | 17 | 17 | 22 | 17 | 4 | 4 |

*Table 3. The number of samples measured for the diameter per group per donor.*

## Histology

The micro pellets were subjected to overnight staining with a solution of 50% eosin in 4% formaldehyde within the Eppendorf tubes as part of the histological preparation. Subsequently, the pellets were embedded in an alginate gel to avoid losing samples during the embedding process. Subsequently, the samples were dehydrated through a series of ethanol steps going from low to high concentration, xylene, and eventually paraffin as mentioned in protocol 6 (page 8 of 'Laboratory Protocols). The samples were then cut with a microtome (Leica Histocore biocut, 14061756235) in 5 µm slices. To ensure the presence of the micro pellets in the gathered slides, the slides were assessed

under the microscope during the cutting process. The stained slides were imaged under an Olympus BX 43 microscope.

**Safranin-O / fast green staining**

To visualize the glycosaminoglycans (GAG) content of the micro pellets a safranin-O (SAF-O) staining was performed. SAF-O stains GAGs varying shades of red. To enhance contrast, fast green is utilized as a counterstain, which imparts a green color to the surrounding tissue. The staining was performed following protocol 7 (page 9 of 'Laboratory Protocols). The samples were rehydrated by xylene, a series of ethanol steps going from high to low concentration, citrate buffer to remove the alginate gel, and lastly demi water. Subsequently, the samples were stained with Weigert's hematoxylin for five minutes, ran in tap water for 10 minutes and one quick change of demi water, counterstained with 0.4% aqueous fast green solution for 4 minutes, washed with two changes of 1% acetic acid for 5 minutes, and eventually stained with 0.125% aqueous SAF-O for 5 minutes. To preserve the sample and the staining, the samples were dehydrated once more with a quick 90% ethanol, 100% ethanol, and xylene series and then coverslipped in Eukitt Quick-hardening mounting medium (03989 Sigma-Aldrich).

**Toluidine blue staining**

Toluidine blue staining was applied to visualize the GAG content within the micro pellets. Toluidine blue stains nucleic acids blue, and GAGs purple due to high affinity towards the sulfurs present in cartilage. In comparison, SAF-O has lower affinity towards these sulfurs and will stain less intensely (27). Similar to the SAF-O staining, a fast green staining served as a counterstain to provide contrast and highlight the GAG content in the surrounding tissue. As described by protocol 8 (page 10 of 'Laboratory Protocols), the samples were rehydrated. Afterward, the samples were stained with 0.4 % toluidine blue, washed with 3 changes of demi water, stained with 0.2% fast green solution, and washed with 2 changes of demi water. Again, the samples were dehydrated, and coverslipped.

**Collagen II immunohistochemistry**

Collagen II is the predominant collagen type found in cartilage and is an important marker for chondrogenesis (28). The presence and distribution of collagen II in the micro pellets was visualized by means of immunohistochemistry (IHC). The samples were rehydrated as stated in protocol 9 (page 11 of 'Laboratory Protocols). The samples were blocked with 0.3% hydrogen peroxide ($H_2O_2$) solution for 10 minutes to prevent any background staining. The antigen retrieval was facilitated enzymatically with 30 minutes of 1 mg/ml pronase (11459643001, Roche) and 30 minutes of 10 mg/ml hyaluronidase (H2126, Sigma-Aldrich) at 37 °C. Subsequently, samples were blocked with 5% PBS-BSA for 30 minutes at room temperature, and incubated with the primary antibody, collagen type II mouse monoclonal antibody (DSHB, II-II6B3), in a concentration of 0.6 µg/mL in 5% PBS/BSA at 4 °C overnight. The next day, the secondary antibody, BrightVision HRP-anti-mouse IgG (151220, Immunologic), was incubated at room temperature for 30 minutes. Following, the samples were incubated in '3 diaminobenzidine (DAB) peroxidase substrate solution (SK-4100, Vector Laboratories) for 2-10 minutes. When brown coloration started to appear, the incubation was stopped by rinsing the samples in milli-Q. Mayers hematoxylin was used as a counterstaining. The timing depended on the strength of the solution, in general 20 seconds or less was necessary. Afterwards, the samples were run in tap water for 10 minutes. In between steps, the samples were washed with 0.1% PBS0-Tween20 (PBS-T) unless otherwise specified. Lastly, the samples were dehydrated and coverslipped. Each histological staining included a known chondrogenic pellet as a positive control.

## Statistical analysis

A two-way ANOVA with a Tukey post hoc test was performed to calculate if any significant differences were present between the average diameters of the experimental micro pellet groups of the four different donors. A P-value of > 0.05 was deemed significant. A nonlinear line regression, with extrapolation to X = 0, was conducted to analyze if the cell number per micro pellet influences the diameter of the micro pellets. The calculations were performed in the software GraphPad Prism 10.

# Results

## Pilot study

The PDMS microwells effectively generated micro pellets in the designated culture period. Appendix 3 illustrates the two extremities in terms of cell number per pellet, with group 1 (1500 cells per pellet) representing the least and group 6 (36000 cells per pellet) the most.

Various timepoints were evaluated with histology. The SAF-O staining illustrated that no GAGs were detected in group 6 (36000 cells per pellet) on day 7, 14 and 22 (Figure 8). Notably, Figure 8 depicts an absence of red staining on day 28-30, while evident red staining is observed in the pellet core in Figure 13. This exemplifies intradonor variability, as Figure 8 and Figure 13 represented two distinct samples from the same donor at the same timepoint. Group 1 (1500 cells per pellet) depicted a consistent absence of red staining across all timepoints. Regrettably, the micro pellets of day 7 were not retrievable due to their small size. The SAF-O results were corroborated by the toluidine blue staining, which revealed the absence of GAGs in both groups, at all assessed timepoints as well (Figure 9).

In contrast, the collagen II IHC staining revealed the presence of collagen II in group 6 at, day 14, day 22, and day 28, and in group 1 at day 28. The brown staining was present in the center of the micro pellets of group 6, day 14, and group 1, day 28. The location of the brown staining was homogeneously distributed in group 6, day 22 and 28 (Figure 10).

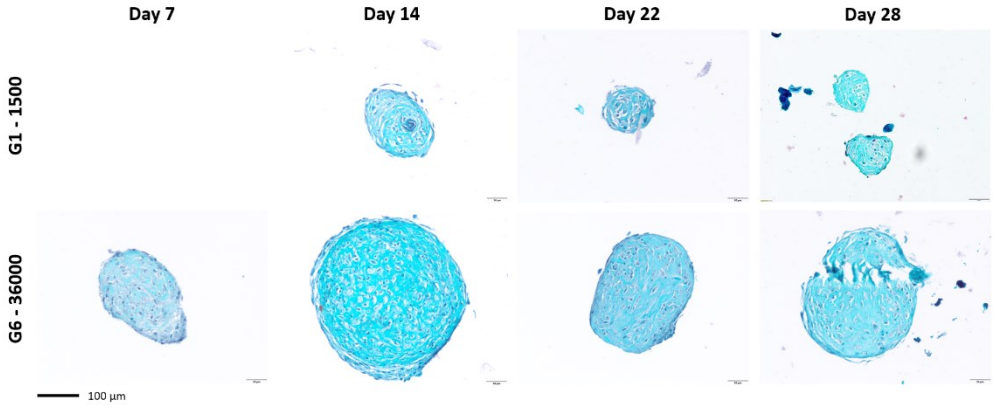


*Figure 8. SAF-O staining of micro pellets from donor C collected at four different timepoints. G1 and G6 represent group 1 (1500 cells/pellet) and group 6 (36000 cells/pellet) respectively. Microscopic images were taken at a 20x magnification, with a scalebar of 100 µm.*

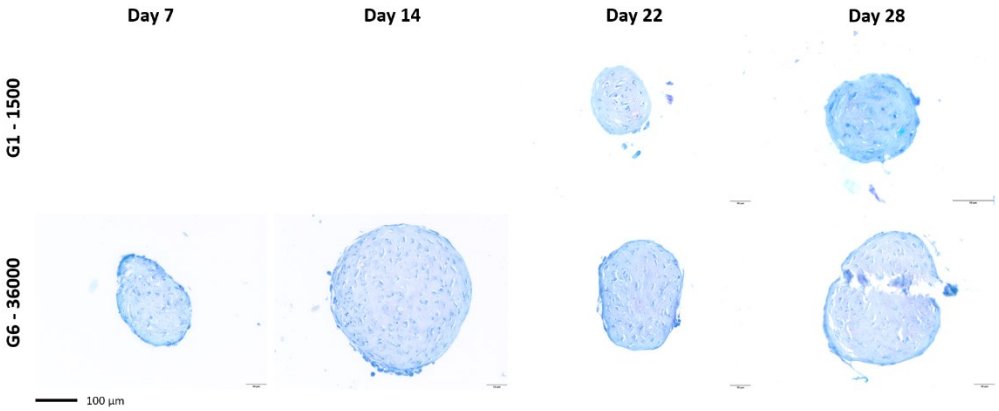


*Figure 9. Toluidine blue staining of micro pellets from donor C collected at four different timepoints. G1 and G6 represent group 1 (1500 cells/pellet) and group 6 (36000 cells/pellet) respectively. Microscopic images were taken at a 20x magnification, with a scalebar of 100 µm.*

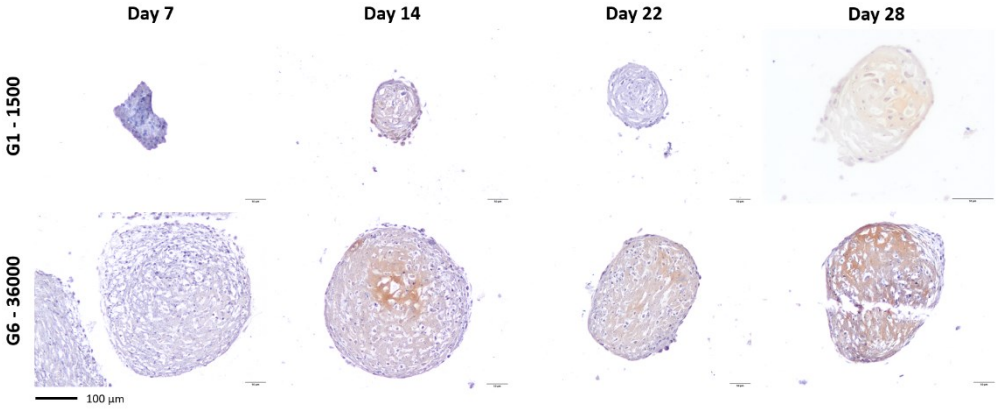


*Figure 10. Collagen II immunohistochemistry staining of micro pellets from donor C collected at four different timepoints. G1 and G6 represent group 1 (1500 cells/pellet) and group 6 (36000 cells/pellet) respectively. Microscopic images were taken at a 20x magnification, with a scalebar of 100 µm.*

## Micro pellet diameter

The diameter of the micro pellets was measured after fixation. Figure 11 provides a representation of the average diameter and SD of each group for every donor. As expected, a trend was visible, with increasing cell numbers per pellet, the diameter of the micro pellets increased. The average diameter of the groups composed of fewer cells, group 1 to 3 (1500, 3000, and 6000 cells/pellet, respectively), did not increase much with each doubling of the cell count per pellet. The groups composed of a higher number of cells, 4, 5, 6, and 7 (12000, 24000, 36000, and 50,000 cells per pellet, respectively), increased more in pellet diameter with each subsequent increase of cells per pellet.

It was notable that the diameters of the micro pellets within groups 4, 5, and 6 (12000, 24000, and 36000 cells per pellet respectively) exhibited considerable variance. These micro pellets exhibited a tendency to aggregate in the microwells, resulting in the notably larger SD (Figure 11) (Appendix 4). Group 3 of donor A also exhibited variance. This group did not form the expected spherical pellets and instead formed loose cellular aggregates (Appendix 4). This atypical formation led to substantial variations in both size and shape.

In Figure 11, the statistical differences in micro pellet diameter between the groups of the donors A, B, and D was illustrated as well. The groups 1 to 5 (1500, 3000, 6000, 12000, and 24000 cells/pellet, respectively), demonstrated a difference in diameter size between donors A and D. The micro pellets

of donor D were at least averagely 200 µm bigger than the micro pellets of donor A in all aforementioned groups. Group 4 showed a similar contrast between donors A, B and D and group 5 between donors B and D. In contrast, group 6 and 7, and the control did not vary in diameter size between donors. Interestingly, there seemed to be a trend visible in Figure 11 that suggests that the micro pellets from the elderly donor A (age >70) tended to be smaller in comparison to those from the younger donors, B and D (age < 20), however the differences did not reach statistical significance between donor A and B.

Lastly, a linear regression was performed to analyze if the number of cells per pellet influences the size of the micro pellets. Overall, the variance in Y, size in µm, was explained by the variation in X, cells per pellet, for 32%, 52%, and 37% for donor A, B, and D, respectively. A linear trend appeared to be present between the micro pellet size and the number of cells per pellet. Theoretically, this trend would pass through zero; however, this was not the observed outcome (Figure 12).

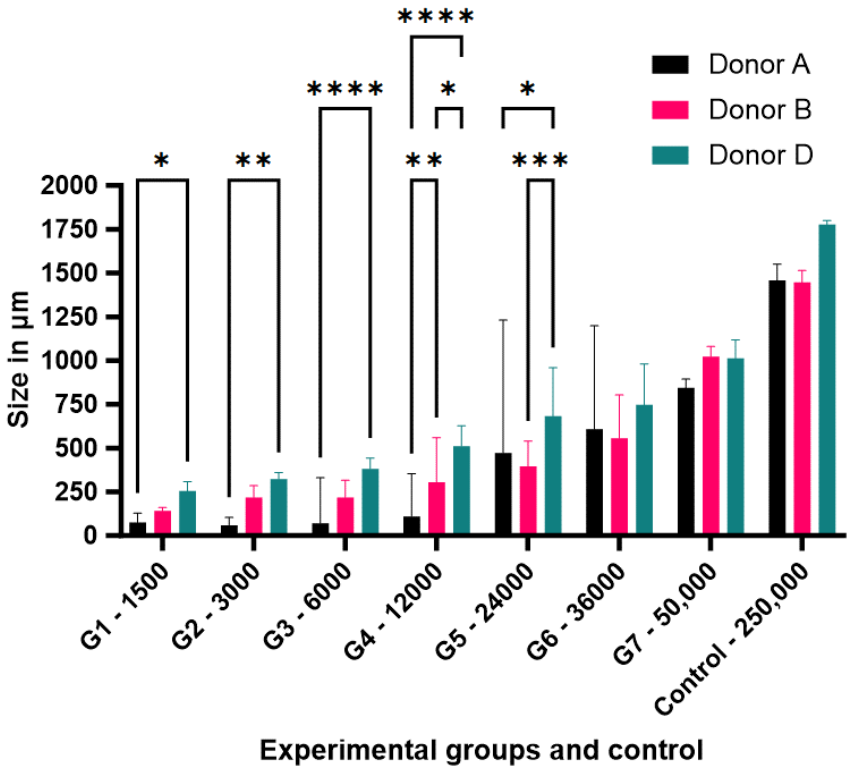


*Figure 11. Graph depicting the average size of the micro pellets of the experimental and control groups of donors A, B and D in µm. A multiple comparisons test results between donors is shown. * 0.05, ** 0.01, *** 0.001, **** <0.0001.*

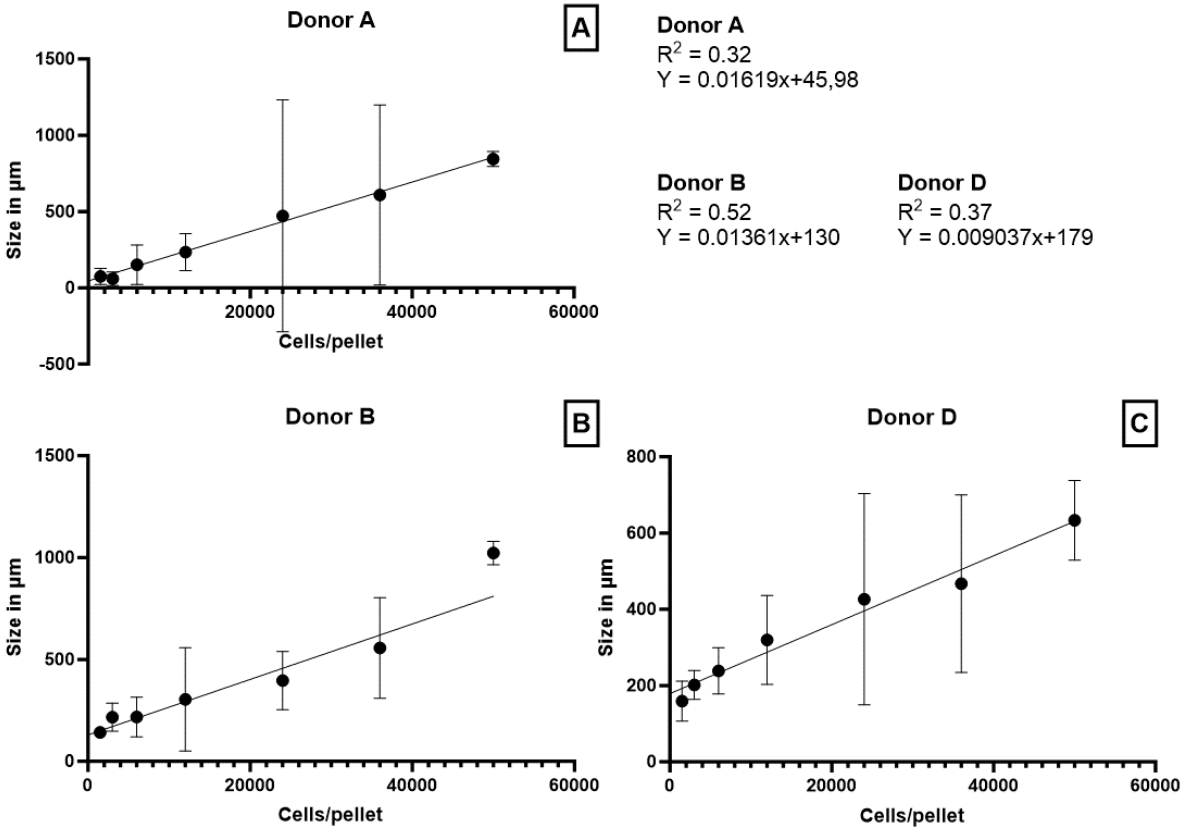


*Figure 12. Linear regression of the size of the micro pellets in µm versus the number of cells per pellet. In graph A, donor A is depicted, in graph B donor B, and in graph C donor D. For each donor the R squared, and function is specified.*

## Histology

The chondrogenic potential of the micro pellets was evaluated with a SAF-O, toluidine blue, and col II staining as described in the methodology section. The detection of GAGs and collagen II suggests that the micro pellets have effectively undergone chondrogenic differentiation.

### SAF-O

The SAF-O staining of the control groups (group 8, 250,000 cells per pellet) of donor A, B, and D consistently revealed a distinct red staining. This red staining indicated the presence of GAGs within the macro pellets and thereby suggested the successful chondrogenic differentiation of the macro pellets. The staining was particularly concentrated in the central regions of the pellets and gradually decreased towards the periphery of the pellets (Figure 13).

The distinctive red staining was also observed in several experimental groups: groups 4, 5, 6, and 7 (12000, 24000, 36000, and 50,000 cells per pellet, respectively) from donors B and D, groups 5, 6, and 7 (24000, 36000, and 50,000 cells per pellet, respectively) from donor A, and group 2 from donor C. In contrast, a subtle pink hue was discernible in group 5 and 6 (24000 and 36000 cells per pellet, respectively) from donor C and group 3 (6000 cells per pellet) from donor D.

Notably, this staining was predominantly evident in groups that aggregated and micro pellet groups characterized by a higher cell count per pellet, specifically groups 4, 5, and 6 (12000, 24000, and 36000 cells per pellet, respectively), and is less pronounced in the micro pellet groups with a lower cell count per pellet, groups 1, 2, and 3 (1500, 3000, and 6000 cells per pellet, respectively). Furthermore, the red staining is more prevalent in groups derived from younger donors in comparison to those from

older donors. Specifically, group 4 (12000 cells per pellet) exhibited positive staining in the younger donors, B and D, in contrast to the older donors, A and C. Group 5 and 6 (24000 and 36000 cells per pellet, respectively) revealed an similar pattern between donors B and D in contrast to donor C (Figure 13).

### Toluidine blue

The chondrogenic differentiation in the control macro pellets was further confirmed by the toluidine blue staining. The purple staining was once more concentrated in the central region (Figure 14).

The results obtained from the toluidine blue staining align closely with those from the SAF-O staining, except for group 4 (12000 cells per pellet) from donor D. This group showed negative results for GAGs with toluidine blue staining but positive results with SAF-O staining. Within the experimental groups, purple staining was observed in groups 5, 6, and 7 (24000, 36000, and 50,000 cells per pellet, respectively) derived from donors A, B, and D. Additionally, groups 1 and 4 (1500 and 12000 cells per pellet, respectively) from donor B exhibited the identical purple staining. A subtle purplish hue was detected in groups 4, 5, and 6 (12000, 24000 and 36000 cells per pellet, respectively) from donor C (Figure 14).

Furthermore, in alignment with the previous SAF-O staining outcomes, all groups that aggregated, 4, 5, and 6 (12000, 24000 and 36000 cells per pellet, respectively), from the respective donors, A, B and D, exhibited positive staining patterns. The difference in positive toluidine blue staining observed between young and old donors reflected the results obtained with SAF-O staining, apart from group 4 (12000 cells per pellet) of young donor D.

### Col II

Chondrocytes secrete collagen II, which is a pivotal marker for in vitro chondrogenesis (28). The presence of collagen II in the control macro pellets was revealed through a collagen II IHC staining, providing evidence of chondrogenic differentiation (Figure 15).

It is noteworthy that collagen II was discerned in groups where there was an absence of red or purple staining in the SAF-O and toluidine blue staining respectively. Specifically, groups 4, 5, 6, and 7 (12000, 24000, 36000, and 50,000 cells per pellet, respectively) from donors A, B, and D exhibited a brown staining pattern, primarily localized in regions that were consistent with the GAG staining's. However, group 3 (6000 cells per pellet) exhibited brown staining in donors B, C, and D, while not showing a corresponding presence of GAGs. A similar trend was observed in group 4 (12000 cells per pellet) from donor A, group 2 (3000 cells per pellet) from donor B, and group 1 (1500 cells per pellet) from donor C (Figure 15).

Once more, the brown staining consistently aligned with the previous outcomes of the SAF-O and toluidine blue staining in regard to the groups that aggregated, groups 4, 5, and 6 (12000, 24000 and 36000 cells per pellet, respectively) of donors A, B, and D. The contrast between the young and old donors disappeared with the collagen II staining. Collagen II was detected in more overlapping groups of the donors, specifically in group 4 (12000 cells per pellet), group 3 (6000 cells per pellet) (excluding donor A), and group 2 (3000 cells per pellet) (excluding donors A and D) (Figure 15).

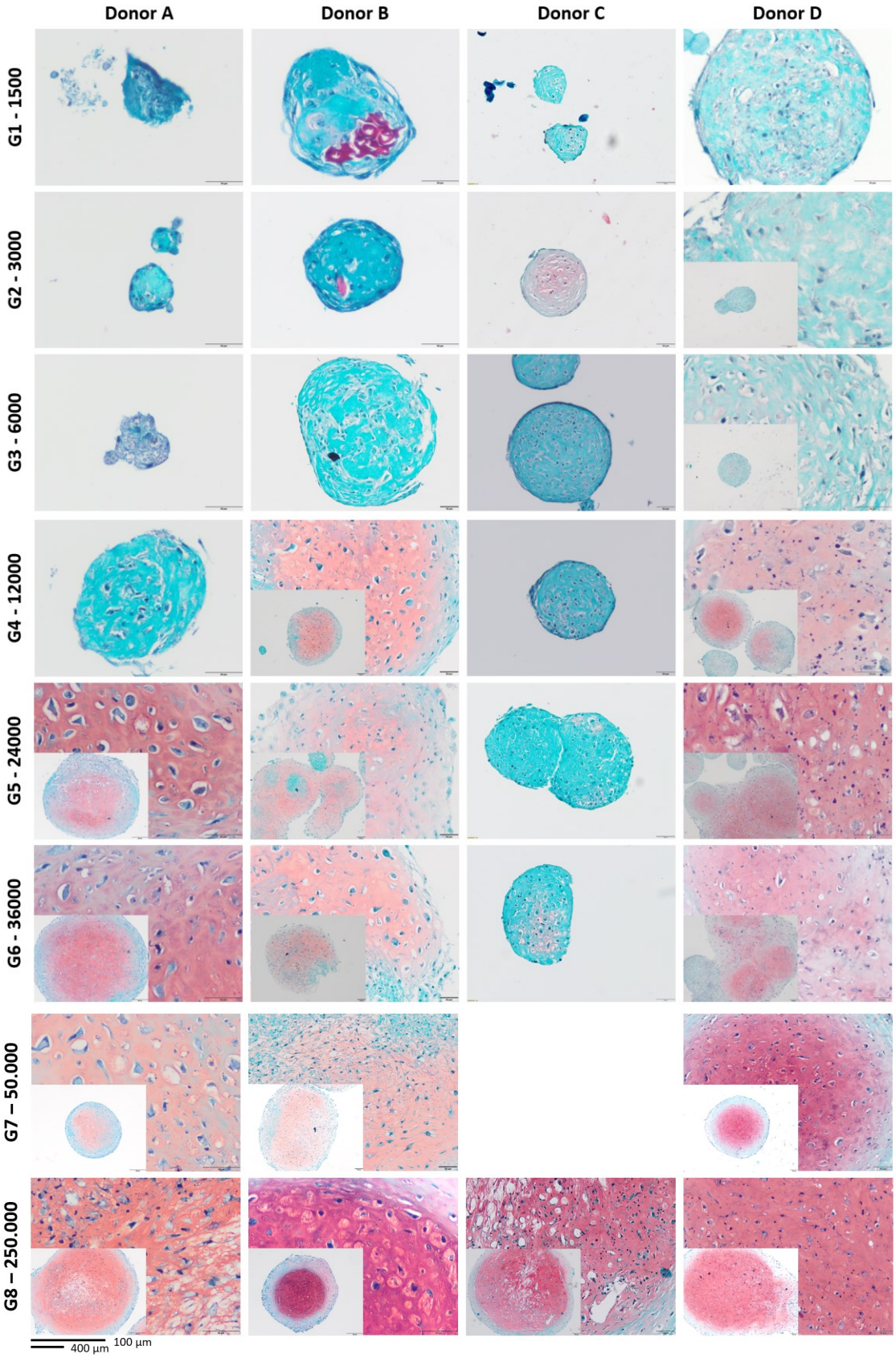


*Figure 13. Complete overview of the SAF-O staining of donors A, B, C, and D. G1-G7 represent the different groups with varying cell densities per pellet: G1 (1500 cells/pellet), G2 (3000 cells/pellet), G3 (6000 cells/pellet), G4 (12000 cells/pellet), G5 (24000 cells/pellet), G6 (36000 cells/pellet), and G7 (50,000 cells/pellet). G8 corresponds to the control group (250,000 cells/pellet. Microscopic images were captured at a 20x magnification, with a scale bar of 100 µm in the larger images. In the smaller pictures in the left corner, the magnification was set at 4x, and the scale bar measured 400 µm.*

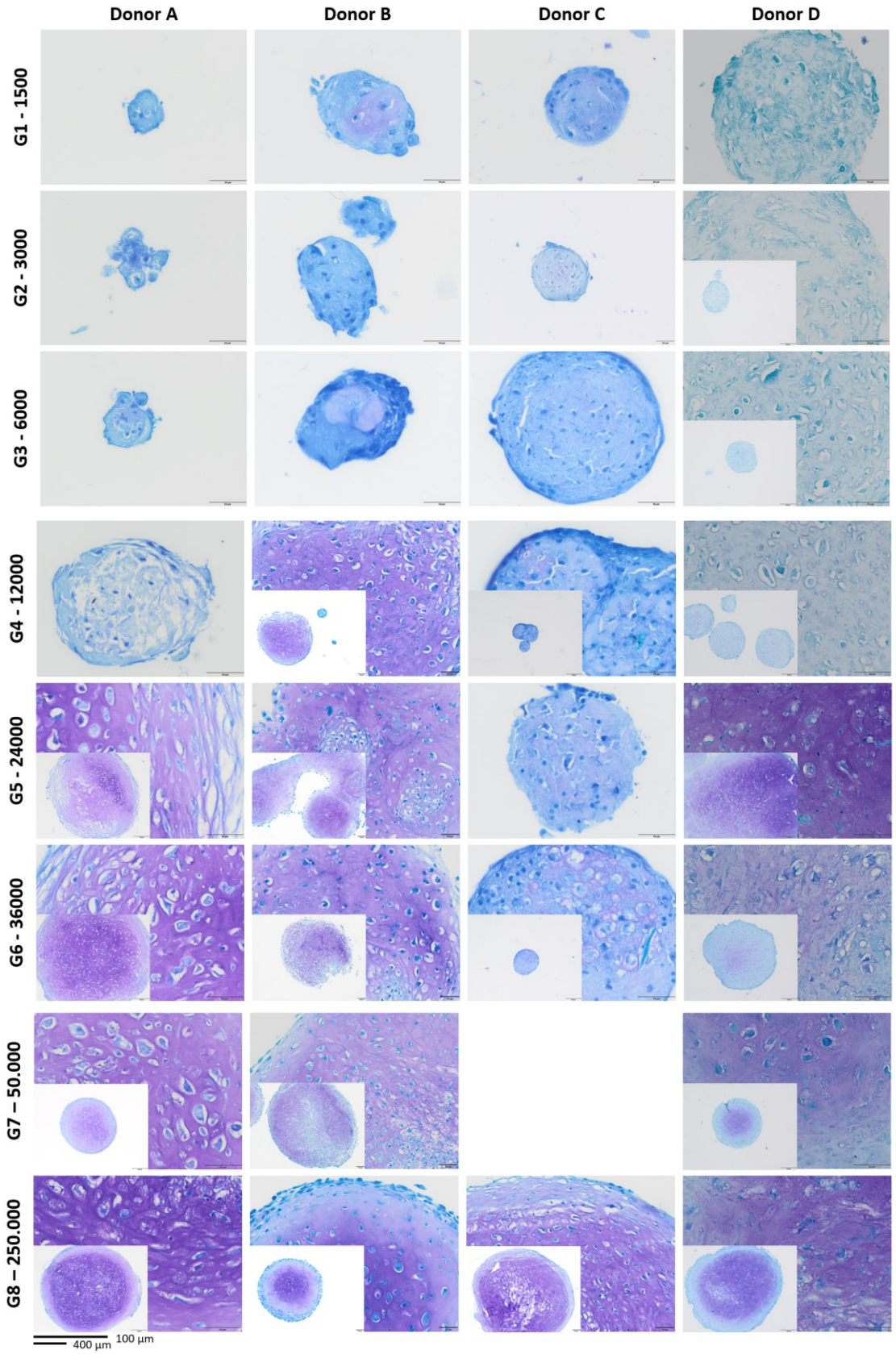


*Figure 14. Complete overview of the toluidine blue staining of donors A, B, C, and D. G1-G7 represent the different groups with varying cell densities per pellet: G1 (1500 cells/pellet), G2 (3000 cells/pellet), G3 (6000 cells/pellet), G4 (12000 cells/pellet), G5 (24000 cells/pellet), G6 (36000 cells/pellet), and G7 (50,000 cells/pellet). G8 corresponds to the control group (250,000 cells/pellet. Microscopic images were captured at a 20x magnification, with a scale bar of 100 µm in the larger images. In the smaller pictures in the left corner, the magnification was set at 4x, and the scale bar measured 400 µm.*

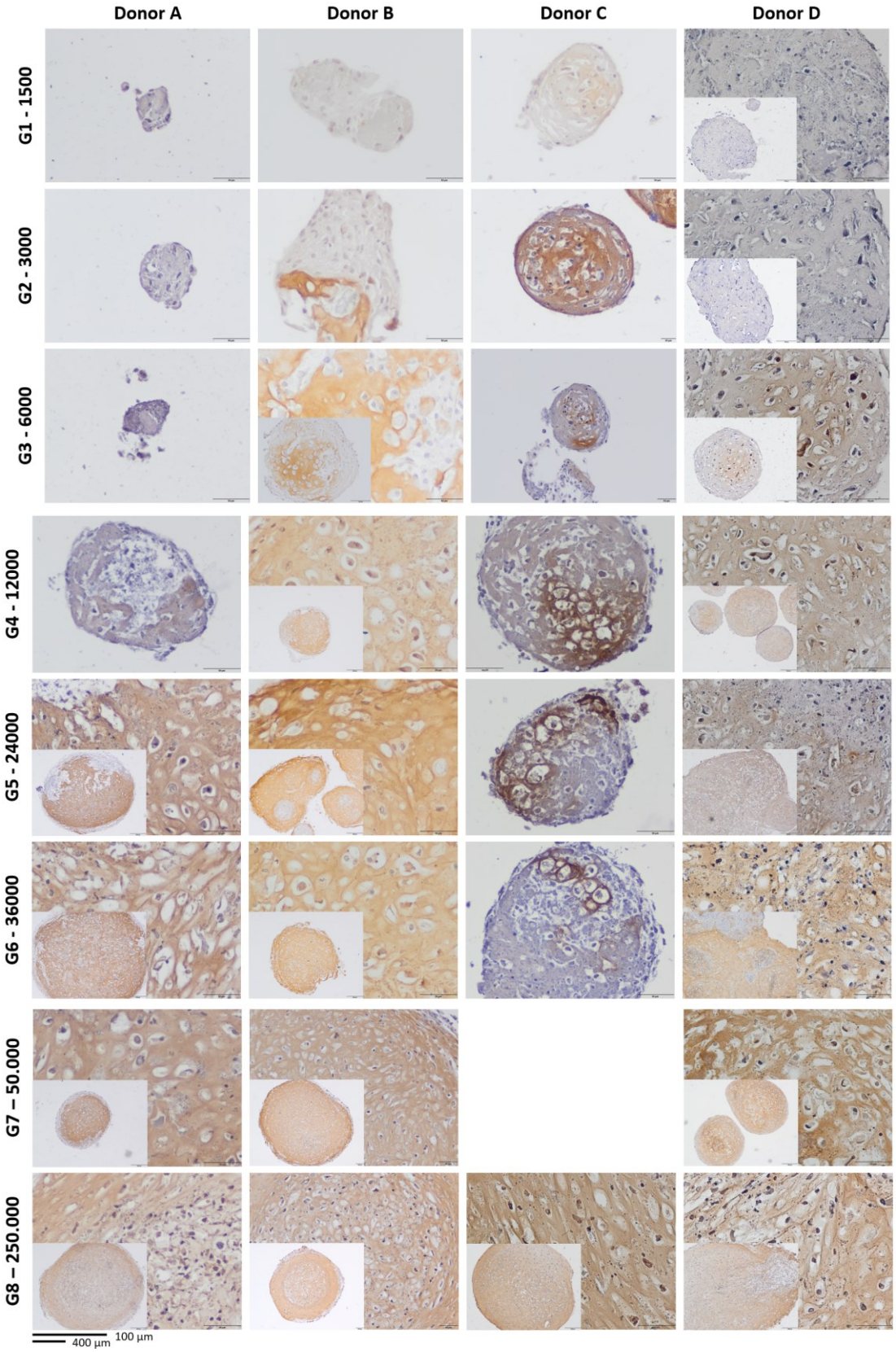


*Figure 15. Complete overview of the collagen II immunohistochemistry staining of donors A, B, C, and D. G1-G7 represent the different groups with varying cell densities per pellet: G1 (1500 cells/pellet), G2 (3000 cells/pellet), G3 (6000 cells/pellet), G4 (12000 cells/pellet), G5 (24000 cells/pellet), G6 (36000 cells/pellet), and G7 (50,000 cells/pellet). G8 corresponds to the control group (250,000 cells/pellet. Microscopic images were captured at a 20x magnification, with a scale bar of 100 µm in the larger images. In the smaller pictures in the left corner, the magnification was set at 4x, and the scale bar measured 400 µm.*

# Discussion and conclusions

In part 2 of this thesis the aim was to generate micro pellets in a range of sizes and study the effect of donor age and cell number per micro pellet on the chondrogenic differentiation potential. Micro pellets have been made before with different microwell systems, and different cell types (21,29–32). In this experiment, BM-MSCs were used to generate micro pellets, which were chondrogenically differentiated in PDMS microwells over 28 days.

The pilot study demonstrated that the microwells supported the formation and collection of micro pellets composed of a range of cell densities. After differentiation in chondrogenic media, the micro pellet cells displayed morphology characteristic of chondrogenesis, with round cells situated in lacunae comparable to the cartilage shown by Hu et al. (33). Unexpectedly, SAF-O and toluidine blue stained negative in a majority of the samples, revealing a discrepancy between the chondrogenic morphology and the GAGs present in the micro pellets. This might be explained by the age of donor A. Donor A is considered an old donor (age > 70) and aged hMSCs can have a decreased chondrogenic potential as shown by Kanawa et al. (34). However, the control macro pellets did show the presence of GAGs. Therefore, the low cell number per micro pellet might have hindered sufficient cell-to-cell contact, potentially affecting robust GAG production in the micro pellets (35,36). Interestingly, the collagen II IHC did yield positive staining in the micro pellets. It could be that the old age of donor A influenced the GAG to collagen II production ratio (28,37).

Following the pilot study, three additional donors, A, B, and D, were used for micro pellet culture. Overall, a few trends were apparent in the results. To start, it has been argued in literature that larger pellets contain inhomogeneous ECM coverage in relation to components such as GAGs and collagen II. Necrotic cores were also reported in some studies (38,39). In addition, Sarem et al. (40) demonstrated that the number of cells in a pellet or spheroid influences the chondrogenesis. A lower number of cells initiated chondrogenic differentiation and accelerated the process as well. It is important to note, however, that the cell seeding density ranged from 70,000 to 500,000 in their experiment (40). Hence, based on literature, smaller pellets seem to be favorable.

However, in our study, the control groups did not contain necrotic cores and showed homogenous coverage of collagen II over the complete area of the pellet. In contrast, the GAGs were primarily concentrated in the center of the pellet and lacked at the periphery. Our results were line with Lam et al. (41), who also observed collagen II more prominently at the periphery and GAGs in the center of hMSC pellets with high matrix production. In this experiment, the micro pellets from group 4 to 7 (12000, 24000, 36000 and 50,000 cells per pellet respectively) showed homogenous GAG and collagen II formation similar to control groups. Unexpectedly, with a lower cell count per pellet, the distribution of GAGs and collagen II was irregular or not present. This could be influenced by the oxygen tension in the micro pellets with a lower cell number. Studies have shown that hypoxia is important for chondrogenic differentiation of MSCs (39,42). It is likely that the micro pellets that remained small enough to stay within the range of oxygen diffusion (approximately 200 µm) did not experience hypoxia, or the exposure to normoxic oxygen conditions inhibited the micro pellets, resulting in less chondrogenesis, while larger micro pellets in groups 4 to 6 (12000, 24000, and 36000 cells per pellet respectively), as well as group 7 (50,000 cells per pellet), appeared to have experienced hypoxia (43).

It is worth noting that the lack of GAGs in group 1 to 3 (1500, 3000, and 6000 cells/pellet respectively) in all groups contradicts the findings of Futrega et al. (32). In their study, micro pellets containing 5000 cells/pellet were cultured with TGF-β exposure which resulted in chondrogenic differentiation after 21 days. Furthermore, the micro pellets performed just as well as the macro pellets, containing 2 *

$10^5$ cells, that were used as a control. Interestingly, they used BM-MSCs for the micro pellets that were cultured in 2% oxygen. In another study, De Moor et al. (29) cultured micro pellets consisting out of 315 cells/pellet and observed the presence of GAGs at day 28. With a different cell type, periosteum-derived MSCs, Nilsson Hall (44) generated micro pellets consisting of approximately 250 cells per pellet and observed low GAG deposition at day 21. However, when the micro pellets were implanted into a critical sized defects of immunodeficient mice, the pellets facilitated full bridging of the defect in four weeks (44). In contrast, to the normoxic oxygen conditions of the previous papers, Markway et al. (39) cultured micro pellets consisting of 170 cells per pellet at a low oxygen tension and saw GAG and collagen II deposition just after 14 days. Berneel et al. (31) identified similar results with fibro chondrocyte micro pellets at low oxygen tension.

Overall, in literature, there are conflicting reports regarding the chondrogenic potential of micro pellets. This highlights the complexity of optimizing chondrogenic micro pellet cultures. While lower cell numbers seem to be more favorable for chondrogenesis, the presence of GAGs and collagen II in micro pellets seems to vary depending on multiple factors, including cell type, oxygen tension, and specific experimental conditions, such as the microwell system. These findings emphasize the need for further research to refine the use of chondrogenic micro pellets as a method for bone regeneration. It is important to standardize the field to achieve more consistent and effective outcomes that can be better compared.

The second trend to be discussed is related to the size of the micro pellets. As anticipated, the number of cells per micro pellet dictates the size of the micro pellets to a certain extent. The calculated line illustrated that the relationship between X (cell density) and Y (the diameter of the micro pellet) was seemingly linear. However, approximately 70% of the variance in Y could not be explained by X, except for donor B which showed a 50% correlation. This goes to show that there are other significant factors that play a role in determining the size of the micro pellets. Murphy et al. (45) drew a similar conclusion when comparing the measured radius to the expected calculated radius of pellets, which was calculated with the number of cells per pellet among other factors. Interestingly, they found a correlation in the smallest group which was composed of 15000 cells per pellet. However, this correlation was not found in their other two groups, which contained 30,000 and 60,000 cells per pellet, respectively, as these pellets had larger radii than expected. The conclusion that was taken from this experiment was that the packing density of the cells decreased when pellets became bigger in size (45). This phenomenon could explain the minimal correlation between the size of the micro pellets and the number of cells per pellet.

Furthermore, Lam et al. (41) discovered that small hMSC aggregates compacted more than large aggregates. This ties into the difference in packing density between small and large pellets. In their collagen II staining, they found collagen II deposited in the center of these pellets which they linked to more contractile cells. They detected that collagen II in larger aggregates was mostly deposited along the periphery of the pellets and GAGs in the center (41). This was not the case for the smaller aggregates, which was mirrored in the results of this experiment. However, the aggregated micro pellets within groups 4 to 6 (12000, 24000, and 36000 cells per pellet, respectively) introduced a notable variation in the mean size of the micro pellets and acts as a confounding factor. As a result, it is imperative to repeat the experiment to establish whether, in addition to cell density, other factors like cellular contraction and packing density exert a substantial influence in determining the size of the micro pellets.

The final trend that was observed in this study was that the age of the donors had an impact on the chondrogenic differentiation and size of the pellets. The results showed that there was a variation among the donors, with significant differences between the old (age > 70) and the young donors (age

< 20) (donor A and C versus donor B and D respectively). The differences between the donors were particularly noticeable in groups 1 to 4 (1500, 3000, 6000, and 12000 cells per pellet respectively), which were smaller in size compared to the young donors. Moreover, group 4 (12000 cells per pellet) of the old donors showed little to no GAGs and collagen II deposition, unlike group 4 of the young donors. While these differences could be attributed to donor variability (41), previous studies have shown that older donors tend to deposit less matrix upon chondrogenic differentiation with a decline in chondrogenic potential (34,46). Therefore, it would be optimal to use a younger donor for future experiments.

Additionally, due to the difficulties with the micro pellet culture, the lack of chondrogenic differentiation and the unwanted aggregation, macro pellets were considered for the subsequent formulation of a bioink. In this study, the macro pellet controls chondrogenically differentiated successfully and consistently, among all donors. Given the large diameter of the macro pellets, they could be crushed to a powder prior to incorporation in to the bioink. This would make the bioink extrudable and facilitate a uniform distribution of active components throughout the bioink. It was hypothesized that the powder would retain the active components necessary for EBR. Similar to how decellularized ECM (dECM) bioinks have been used to replicate the microenvironment of tissues (47). Jang et al. (47) discovered that a dECM-based bioink construct enhanced cellular function after implantation, which resulted in improved therapeutic outcome.

### Conclusion

Based on the results of this chapter, it was concluded that smaller micro pellets (< 6000 cells per pellet) and a young donor were the preferred choices for the development of bioink incorporating micro pellets. Smaller micro pellets did not demonstrate unwanted aggregation and the chondrogenic differentiation of the micro pellets from younger donors proved to be more successful compared to those from older donors. Consequently, group 3 (6000 cells per pellet) and donor B were selected for subsequent experimentation to formulate a bioink. Group 3 exhibited minimal aggregation, promising morphological characteristics, and clear collagen II deposition. In addition, considering the successful chondrogenesis of the macro pellets, the decision was made to formulate a second bioink with crushed macro pellets.

## Limitations and future directions

The chondrogenic differentiation of the micro pellets was evaluated with a SAF-O, toluidine blue, and col II staining. While these staining's visualize important components of cartilage-like tissue, such as GAGs and collagen II, the data is qualitative. To investigate the relative number of GAGs per DNA present, the quantitative dimethylmethylene blue (DMMB) assay could be performed in the future. Furthermore, a collagen X IHC could be performed to assess signs of hypertrophy in the micro pellets (48).

The culture conditions remained consistent across all culture periods for each donor, except for the collection date which ranged between day 28 to 31. Furthermore, the pilot study lacked an internal control. The control pellets for the pilot study data had been generated a few weeks in advance. In addition, no controls were cultured for the individual analyzed timepoints during the pilot study.

The aggregation issue observed in groups 4 to 6 (12000, 24000, and 36000 cells per pellet, respectively) of donors A, C, and D introduced considerable variation in diameter. The aggregation might have been caused by the partial media exchange that was maintained. The micro pellets from the two young donors seemed to produce more ECM, resulting in larger micro pellets which were

easily dislodged from their individual microwells during media exchange. In contrast, the micro pellets of donor C were difficult to collect and required several washing steps to dislodge.

The aggregation of the micro pellets is a problem that Futrega et al. (18) overcame by the creation of the microwell-mesh. This mesh was applied over the microwells to secure the micro pellets within their designated microwells during media exchange. The micro pellets tended to attach to the mesh and were detached with a cell scraper on the collection day (18). In future micro pellet experiments, it would be advisable to use the microwell mesh to limit unwanted aggregation. In addition, the integration of a microwell mesh could enhance the efficiency of micro pellet collection. As the micro pellets adhere to the mesh, they can be easily dislodged using a cell scraper. A microwell mesh could be produced in-house with melt electro writing (MEW).

In future experiments, micro pellets could be subjected to hypoxic conditions to provide insight into the impact of low oxygen levels on their chondrogenic differentiation. It would be interesting to evaluate whether hypoxia induces the production of GAGs in smaller micro pellets (< 6000 cells per pellet). These micro pellets, with a diameter within the range of oxygen diffusion (approximately 200 μm), typically do not encounter hypoxic conditions during normoxic culture.

# Part 3 – Bioinks

# Methods

## Study design

In chapter 3, the concluding part of the study, the objective was to formulate two bioinks (Figure 16). One incorporating the micro pellets (6000 cells per pellet) into a gelatin methacryloyl (GelMA) solution and the second combining pulverized macro pellets (250,000 cells per pellet) with a GelMA solution. The micro and macro pellets were devitalized prior to formulation of the bioinks. After devitalization, the macro pellets were crushed to a powder with a bead beater.

The bioinks were initially poured into a circular PDMS mold and a flat-bottom 96-well plate. This pilot experiment was conducted to assess the ability of GelMA to form a gel with embedded pellet particles. The resulting constructs were evaluated using the Olympus SZ61 stereomicroscope to ascertain whether the intended shape was achieved.

Subsequently, the functionality of the bioink was tested with a volumetric bioprinter. The bioprinter was employed to produce two distinct shapes: the test 'lemon' shape and the shape of an incus bone. The 'lemon' shape was printed to determine the printability of the bioink and to assess the optimal light dose. Following the identification of the optimal light dose, the incus bone was printed. The shape of an incus bone was selected due to its size, the bone was small enough to be printed entirely, and its complex shape, making it an ideal test specimen. The fabricated constructs were stained with Alcian blue following the printing process and examined under the Olympus SZ61 stereomicroscope. The printed constructs were compared to their models in the original STL files.

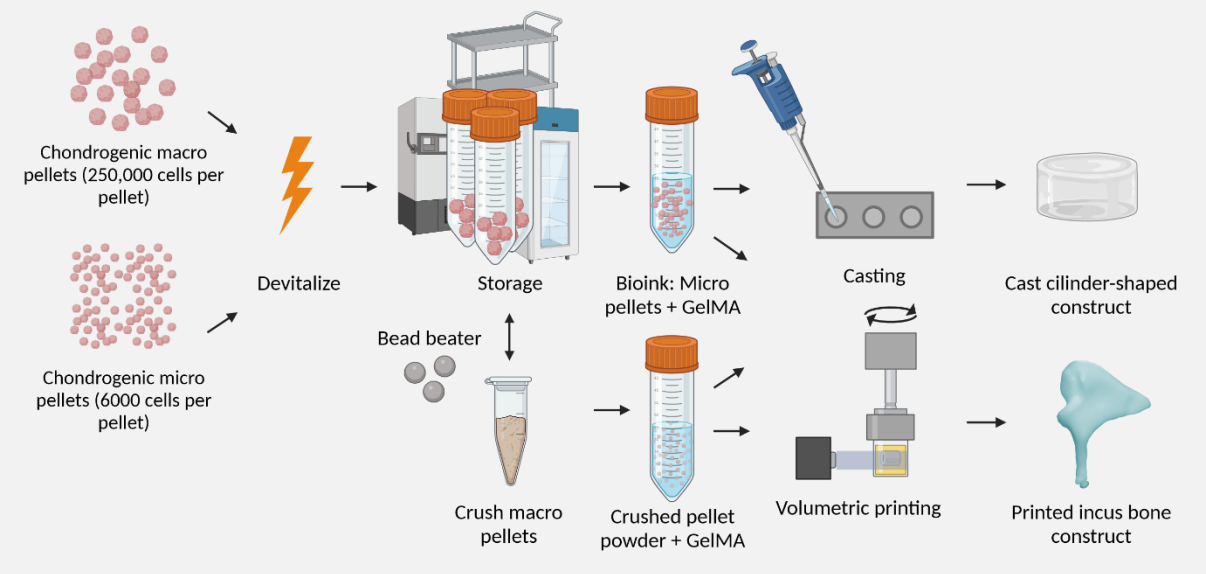


*Figure 16. Overview of the formulation of two bioinks, one composed of GelMA and micro pellets (6000 cells per pellet) and the other composed of GelMA and crushed macro pellet powder, and the subsequent experimentation with the bioinks.*

## Macro and micro pellet culture and chondrogenic differentiation

For the third chapter, the culture of macro and micro pellets was repeated. Six PDMS microwell system wells were positioned in a 6-well plate for the cultivation of approximately 228 micro pellets. Around 70 macro pellets were cultured in a low-attachment round-bottom 96-well plate. Both cultures followed the procedures outlined in the methods of part 2: 'Micro pellets' and protocol 5 (page 7 of 'Laboratory Protocols'). The prior expansion of hMSCs was performed as described in protocol 2 (page 3 of 'Laboratory Protocols').

## Collection and freeze-drying of the macro and micro pellets

After 28 days of culture, the macro and micro pellets were harvested and distributed across multiple Falcon tubes following the guidelines in the methods of part 2: 'Micro pellets' and in protocol 5 (page 7 of 'Laboratory Protocols'). The devitalization process was conducted as described by Longoni et al. (11). Complete removal of the PBS0 in which the micro pellets were collected proved challenging. Consequently, the micro pellets were immersed in as little as possible PBS0, avoiding pellet loss during pipetting, and subsequently subjected to freeze-drying. The freeze-dried pellets were stored in a -80 °C freezer.

## Crushing of the macro pellets

The macro pellets were crushed with zirconium beads (120524-890, Bertin Technologies) in a bead beater (Mini beadbeater™, Biospec products), following protocol 10 (page 13 of 'Laboratory Protocols). Screw-capped microtubes (5082211, Sarstedt) were used to prevent spillage during the bead beating process. These micro tubes were autoclaved in advance for sterility. In a flow hood, 20 macro pellets were added to each micro tube, and zirconium beads were added to fill the tubes halfway (49). After adding the beads, the microtubes were placed on dry ice. The pellets were placed in the bead beater and beating was conducted for 1 minute, followed by cooling for 1 minute on dry ice. This process was repeated three times.

## Formulation of the bioink

### Preparation of the GelMA

The bioink was prepared sterilely with different concentrations of GelMA in a flow hood conform to protocol 11 (page 14 of 'Laboratory Protocols). A 5% and 10% GelMA was made with 50 mg and 100 mg freeze-dried GelMA, which was added to 950 µl and 900 µl 0.1 % LAP (Lithium Phenyl-2,4,6-trimethylbenzoylphosphinate) in PBS0, respectively. The 0.1 % LAP/PBS0 was prepared with a 1 % LAP/PBS0 stock solution. The stock solution was made with 100 mg LAP powder in 10 ml PBS0. The lights in the flow hood were switched off due to LAP's sensitivity to light.

After combining the components, the falcon tube was wrapped in aluminum foil to diminish the light exposure. To ensure the components were fully mixed, the falcon tube was put in a falcon tube spinner in an incubator at approximately 37 °C for 30 minutes. The bubbles that subsequently formed were eradicated by spinning the falcon tube down at 400*g* for 1 minute.

### Incorporation of the micro pellets

The micro pellets were removed from the -80 °C freezer and rehydrated in PBS0, whereafter excess PBS0 was subsequently removed. The rehydrated micro pellets were then incorporated into the prepared GelMA to complete the bioink formulation.

### Incorporation of the crushed macro pellet powder

The powder obtained from the pulverized macro pellets was collected using either PBS0 or 0.1 % LAP/PBS0 solution as stated in protocol 10 (page 13 of 'Laboratory Protocols). One milliliter of the solution was introduced into screw-capped microtubes, after which the contents of the microtubes were transferred to a small petri dish. The beads and microtubes were repeatedly washed with the chosen solution, and consequently gathered in separate Falcon tubes or immediately combined with the freeze-dried GelMA to create the final bioink.

## Casting the bioink

The casting of the bioinks served as preliminary experiment before bioprinting was performed. The casting pilot was performed with the bioink incorporating crushed pellet powder. The bioink contained around 25 crushed macro pellets of donor 56 in approximately 500 µl 10% GelMA. The prepared bioink was cast into a flat bottom 96-well plate and a circular PDMS mold following the steps outlined in protocol 12 (page 15 of 'Laboratory Protocols). The bioinks were kept in an incubator at 37 °C to maintain fluidity, given that GelMA can gelate reversibly at temperatures below 37 °C. When the bioink was removed from the incubator, it was instantly pipetted into the wells. It was crucial to avoid the formation of air bubbles as these could distort the shape of the cast constructs. A control well containing only GelMA was included. Both the wells in the PDMS mold and the 96-well plate were cured for 3 minutes in a UV-oven.

## Volumetrically printing the bioink

Crystal printing vials were filled with the bioink and chilled on ice to ensure the GelMA would thermally gelate. This would facilitate an even distribution of the micro pellets or crushed pellet powder in the bioink in the vials. When the printing vial was placed in the volumetric printer the height of the vial was adjusted to ensure the light projection would hit the vial at the correct location, which was visible on a linked computer. To evaluate the printability of the incus bone shape volumetrically and to assess the level of detail achievable in the construct, 250 µl of 5% GelMA was printed at various light doses—245, 250, 260, and 270 mJ/cm$^2$ (Figure 18).

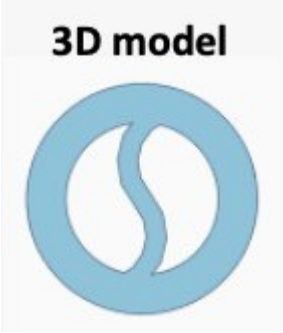


*Figure 17. The shape of the lemon test shape for volumetric printing. The outer ring is 1 mm in diameter and the inner strut 0.5 mm. Courtesy of Paulina Nunez Bernal.*

In the continuing experiment, the bioink containing incorporated crushed pellet powder was tested. The applied bioink consisted of around 65 crushed macro pellets in approximately 5 ml of 10% GelMA, subsequently diluted to 5% GelMA to achieve a higher volume. Initially, a 'lemon' test shape was printed at varying light doses (250, 300, and 500 mJ/ cm$^2$) to assess the bioink's ability to achieve detailed structures, specifically the middle strut (Figure 17). With the most optimal light dose, a triplicate was printed to statistically compare the diameter of the outer ring and middle strut with the original STL file. Subsequently, upon successful printing of the middle strut, the incus bone was printed. The incus bone was printed at different light doses (270 and 300 mJ/ cm$^2$), based on the optimal light dose for the previously printed 'lemon' shape.

*Figure 18. Incus bone shape for volumetric printing. The incus is approximately 6.7 mm in height, 5.2 mm in width, and 1.5 mm in length.*

Following the printing process, the fabricated constructs were rinsed with PBS0 and transferred from the crystal printing vials to a 12-well plate. The constructs were printed and processed according to protocol 13 (page 16 of 'Laboratory Protocols).

## Construct assessment

Both the cast and printed constructs were assessed with an Olympus SZ61 stereomicroscope. The cast constructs were imaged with black background on the tip of a spoon or spatula to ensure that the construct held shape when taken out of PBS0.

The volumetric printed constructs were stained with Alcian blue prior to imaging. The staining duration varied, typically requiring 5 minutes or less, depending on the Alcian blue solution's concentration. Following the staining, the constructs were washed with PBS0, and subsequently imaged in the PBS0 medium to evaluate both the construct's shape and the distribution of the crushed pellets. The outer ring and the inner strut of the triplicate ‘lemon’ shape were measured with Olympus cellSens Entry 4.1.1 imaging software. Measurements were taken at three randomly selected locations on both the outer ring and inner strut, and the averages and SD were calculated.

## Statistical analysis

A two-tailed unpaired T-test was conducted to determine the presence of a significant difference between the average diameter of the volumetrically printed 'lemon' outer ring and inner strut, and their original STL file. A P-value of > 0.05 was deemed significant. The calculations were performed in the software GraphPad Prism 10.

# Results

## Casting

The bioink with crushed pellets was initially evaluated through casting. In **Error! Reference source not found.**, the resulting constructs are displayed. There was a limited number of macro pellets available for crushing in this pilot, which led to a sparse distribution of pellet powder. The crushed donor 56 macro pellets resulted in relatively large individual particles, ranging from approximately 500 to 1400 µm. In the top view of Figure 20, both groups showed singular pellet pieces, reflecting the restricted amount of powder applied in this trial. The constructs held shape when taken out of the molds and when turned on the spatula (**Error! Reference source not found.** side view).

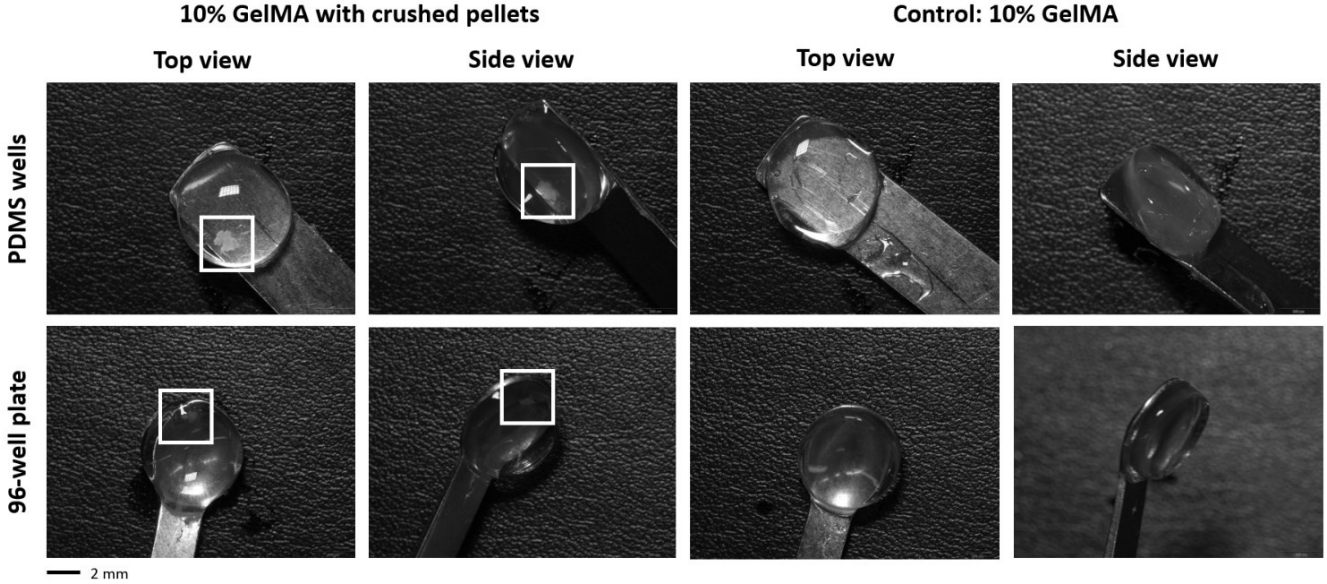


*Figure 19. Cast bioink constructs consisting of 10% GelMA with crushed pellet powder. The white squares highlight the presence of a crushed pellet particle. The microscopic images include a scalebar measuring 2 mm.*

## Volumetric bioprinting

The 'lemon' shape was printed to assess the bioink's ability to crosslink after UV exposure. Different light doses were deployed to evaluate the optimal light dose range. In Figure 21, there is a trend visible, when the light dose increased, the thickness of the outer bands of the lemon increased as well. In Appendix 5, a microscopic overview of the triplicate of the 'lemon' constructs, printed with a light dose of 250 mJ/cm$^2$, is given. Figure 22 illustrates that there is no difference in the measured diameter of the outer ring and inner strut compared to the same features in the original STL file.

The optimal light dose was expected to fall between 250 and 300 mJ/cm$^2$, based on the light doses employed for printing the lemon shape (Figure 21). The incus bone shaped constructs were subsequently printed using a light dose of 270 mJ/cm$^2$. The incus-shape was printed with a light dose of 300 mJ/cm$^2$ as well, to examine whether the details of the incus-shape became more or less defined (Figure 20). Visually, the incus-shape printed with a light dose of 270 mJ/cm$^2$ appeared very similar to the control. In contrast, the incus-shape printed with a light dose of 300 mJ/cm$^2$, visually deviated from the control at the apex of the incus, where an indentation was observed (Figure 22). The particles were distributed evenly, and individually visible, in both constructs. The size of the particles ranged from approximately 4 to 45 µm. In comparison to the original STL file, every incus bone shaped construct visualized in Figure 22 lacked details, such as the lenticular process at the end of the long crus where the incus connects with the subsequent ossicle.

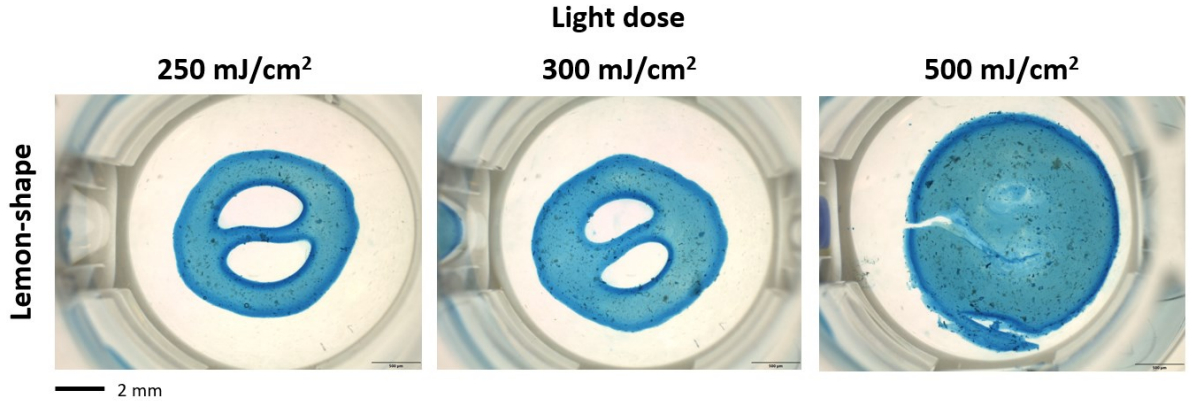


*Figure 21. Volumetrically printed 'lemon' test shapes stained with Alcian blue. Different light doses were used, 250, 300, and 500 mJ/cm². The dark spots in the blue constructs are crushed pellet particles. The microscopic images include a scalebar measuring 2 mm.*

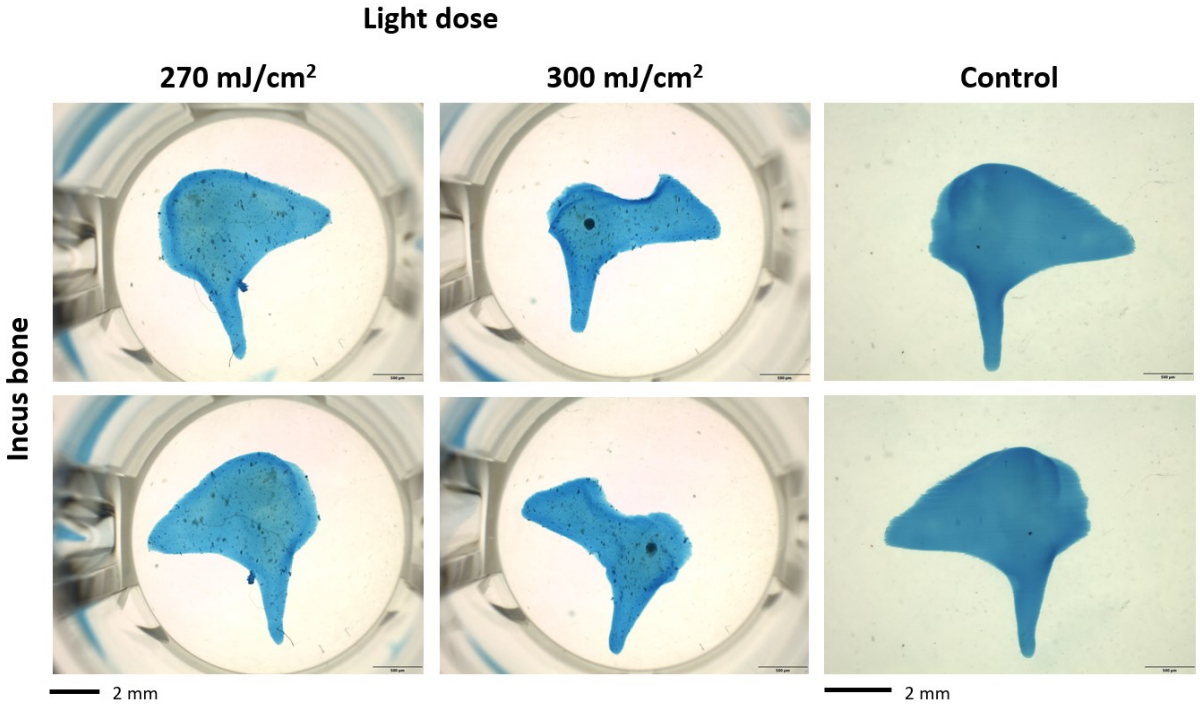


*Figure 20. Volumetrically printed incus bones. Two light doses were used, 270 and 300 mJ/cm². The dark spots in the blue constructs are crushed pellet particles. The control was printed with different light doses as well, 245, 250, 260 and 270 mJ/cm². No visible differences were detected and only one light dose is shown. The light dose for the control was unspecified because the light dose per specific control was unknown; after printing, the controls were not separated for post-processing. The microscopic images include a scalebar measuring 2 mm.*

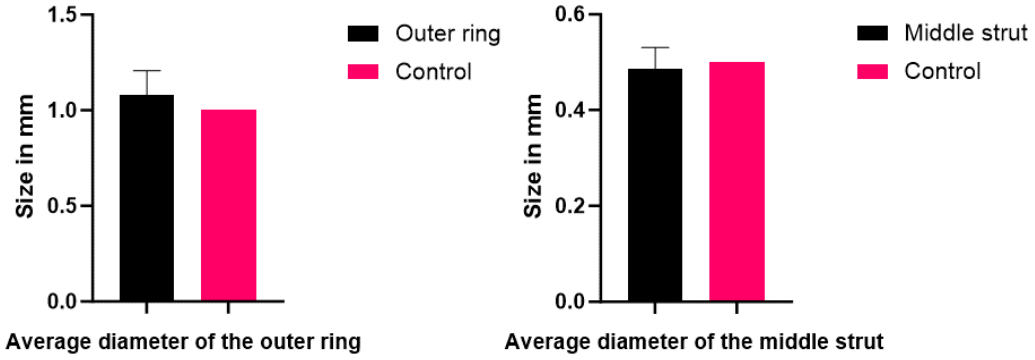


*Figure 22. The average diameter of the outer ring and the middle strut of three 'lemon' shaped constructs printed with a light dose of 250 mJ/cm². The control represents the original size in the STL file, which was 1 mm for the outer ring and 0.5 mm for the middle strut.*

# Discussion and conclusions

In part three of this thesis, the goal was to create and evaluate a bioink composed of chondrogenically differentiated pellets and GelMA. The bioink incorporating micro pellets was not evaluated. However, as a courtesy of Paulina Bernal Nunez, Figure 23 shows that printing with micro pellets should be possible. The bioink mentioned hereafter is composed of crushed macro pellet powder and GelMA.

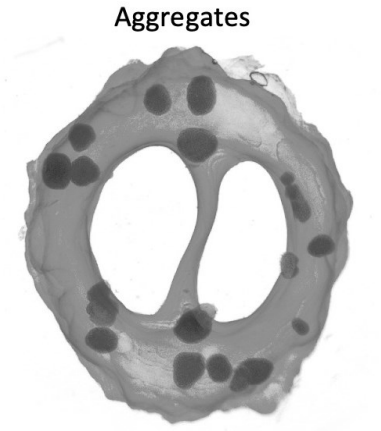


*Figure 23. Volumetrically printed lemon shape composed of GelMA and aggregated cells of a hepatocyte cell line. Courtesy of Paulina Nunez Bernal.*

The printed constructs demonstrated that the integration of macro pellet particles into the GelMA did not visibly impact the printability of the bioink and the shape fidelity of the constructs. It was hypothesized that the incorporation of the macro pellet particles would induce scattering as the particle's ECM is non-transparent and thereby affect shape fidelity (14,17). However, the triplicate of the 'lemon' shape, which were printed with a light dose of 250 mJ/cm², exhibited no variances in outer ring and middle strut diameter when compared to the original STL file. Therefore, it appears that the degree of scattering was relatively minimal.

Nevertheless, despite the successful volumetric printing of the bioink, the printed incus bone shape lacked crucial details compared to the original STL file. Specifically, the lenticular process at the end of the long crus. The absence of these details could be attributed to the fact that the ideal printer settings necessary for the optimal resolution were not established (50). The lenticular process of the incus is 260 µm in diameter, which is the smallest diameter of the incus bone (51). A resolution of 260 µm should be printable with a volumetric bioprinter, as shown by Bernal et al. (15,16) and Loterie et al. (52). It is worth emphasizing that the light dose plays a pivotal role in determining the resolution of the printed constructs. An excessive dose may lead to off target crosslinking within the bioink (15). Furthermore, the diffusion of the chemical components in the bioink could affect the resolution as well (15).

These are all components that warrant consideration in subsequent experiments. Moreover, it would be rational to implement strategies to mitigate the impact of scattering and assess their effect on the construct resolution (14,16).

In our experiment, the density of the macro pellet powder within the cast bioink constructs was notably low. In contrast, in the printed constructs, the particle density was relatively higher with an even distribution through the constructs. Nevertheless, individual particles with various sizes remained visible. To attain and enhance uniform dispersion of the powder within the constructs, a finer particle size should be achieved. Furthermore, the density of the powder in the bioink could be increased in increments to thoroughly explore the crosslinking capabilities of the bioink. Therefore, the reduction of scattering within the bioink could be paramount in following experiments.

To attain a finer powder in future experiments, the use of one 9.5 mm stainless-steel bead is recommended for small samples. Additionally, a cryogenic pulverization process should be employed to ensure the thorough powderization of the pellets (53). Thereafter, the optimal powder density within the bioink should be established.

# Limitations and future directions

The consistency between the cast constructs and the volumetrically print constructs lacked in regard to the bioink formulation. The casts were formulated with 10% GelMA while the printed constructs were made with 5% GelMA. In the future, the goal is to print with different percentages of GelMA, including 10%. Literature indicates that various percentages GelMA have been used for volumetric printing. Gehlen et al. (50) evaluated GelMA concentrations of 2.5 %, 5 % and 10 %. For their application, which involved live cells, a concentration of 5% GelMA was optimal. However, in this study where the bioinks contained dead cells, a 10% GelMA composition, offering higher stiffness and increased stability, might be of interest.

The exact amount of LAP in the cast and printed constructs is unknown because a mistake was made in the calculations for the 1% LAP stock solution, which affected the derivative 0.1 % LAP/PBS solutions that were used in the formulation of the bioinks. It was known that the concentration of the LAP in the 0.1% LAP/PBS solution was below 1%, but in following experiments the concentration should be exact. The LAP concentration is important for the resolution of the fabricated constructs (15,50). There is an inverse relation between the LAP concentration and the light dose needed to crosslink a construct (50).

During the bead beating process, some screw-capped micro tubes cracked due to the stark difference in temperature between the cycles of cooling and beating. It is recommended to look into a different type of plastic screw-capped tube for the bead beating process that can withstand such differences in temperature.

# Final conclusion

This thesis describes the first steps that were taken towards the production of a bioink for EBR. First, a microwell system was established in collaboration with the Inge Zuhorn group in Groningen for the generation of micro pellets. In continuation, the initial stages of micro pellet culture were explored, and the process of optimization started. In the future, micro pellet culture could be investigated as a possible addition or substitution of standard macro pellet culture. In addition, the chondrogenic differentiation of micro pellets could be studied in depth, and the markers and tests for these experiments could be standardized across research groups. Lastly, as a proof of concept, it was demonstrated that a bioink, composed of GelMA and crushed pellet powder, could be formulated and used to 3D bioprint a complex construct – an incus bone.

# References


1. (US) O of the SG. The Basics of Bone in Health and Disease. In: (US) O of the SG, editor. Bone Health and Osteoporosis: A Report of the Surgeon General [Internet]. Rockville: Office of the Surgeon General (US); 2004 [cited 2023 Sep 7]. Available from: https://www.ncbi.nlm.nih.gov/books/NBK45504/

2. Ansari M. Bone tissue regeneration: biology, strategies and interface studies. Prog Biomater [Internet]. 2019 Dec 1 [cited 2023 Sep 7];8(4):223. Available from: /pmc/articles/PMC6930319/

3. Manzini BM, Machado LMR, Noritomi PY, da Silva JVL. Advances in Bone tissue engineering: A fundamental review [Internet]. Vol. 46, Journal of Biosciences. Springer; 2021 [cited 2022 Dec 15]. p. 1–18. Available from: https://link.springer.com/article/10.1007/s12038-020-00122-6

4. Agarwal R, García AJ. Biomaterial strategies for engineering implants for enhanced osseointegration and bone repair. Adv Drug Deliv Rev. 2015 Nov 1;94:53–62.

5. Schmidt AH. Autologous bone graft: Is it still the gold standard? Injury. 2021 Jun 1;52:S18–22.

6. Tsiklin IL, Shabunin A V., Kolsanov A V., Volova LT. In Vivo Bone Tissue Engineering Strategies: Advances and Prospects. Polymers (Basel) [Internet]. 2022 Aug 1 [cited 2023 Jan 31];14(15). Available from: /pmc/articles/PMC9370883/

7. de Silva L, Bernal PN, Rosenberg AJW, Malda J, Levato R, Gawlitta D. Biofabricating the vascular tree in engineered bone tissue. Acta Biomater. 2023 Jan 15;156:250–68.

8. Thompson EM, Matsiko A, Farrell E, Kelly DJ, O'Brien FJ. Recapitulating endochondral ossification: A promising route to in vivo bone regeneration. Vol. 9, Journal of Tissue Engineering and Regenerative Medicine. 2015. p. 889–902.

9. Gerstenfeld LC, Cullinane DM, Barnes GL, Graves DT, Einhorn TA. Fracture healing as a post-natal developmental process: Molecular, spatial, and temporal aspects of its regulation. J Cell Biochem [Internet]. 2003 Apr 1 [cited 2023 Jan 11];88(5):873–84. Available from: https://pubmed.ncbi.nlm.nih.gov/12616527/

10. Shapiro F. Bone development and its relation to fracture repair. The role of mesenchymal osteoblasts and surface osteoblasts [Internet]. Vol. 15, European Cells and Materials. Eur Cell Mater; 2008 [cited 2023 Jan 11]. p. 53–76. Available from: https://pubmed.ncbi.nlm.nih.gov/18382990/

11. Longoni A, Utomo L, Robinson A, Levato R, Rosenberg AJWP, Gawlitta D. Acceleration of Bone Regeneration Induced by a Soft-Callus Mimetic Material. Advanced Science [Internet]. 2022 Feb 1 [cited 2022 Nov 15];9(6). Available from: https://pubmed.ncbi.nlm.nih.gov/34962103/

12. Longoni A, Pennings I, Cuenca Lopera M, van Rijen MHP, Peperzak V, Rosenberg AJWP, et al. Endochondral Bone Regeneration by Non-autologous Mesenchymal Stem Cells. Front Bioeng Biotechnol. 2020 Jul 9;8.

13. de Silva L, Longoni A, Staubli F, Nurmohamed S, Duits A, Rosenberg AJWP, et al. Bone Regeneration in a Large Animal Model Featuring a Modular Off-the-Shelf Soft Callus Mimetic. Adv Healthc Mater [Internet]. 2023 [cited 2023 Oct 23]; Available from: https://pubmed.ncbi.nlm.nih.gov/37580174/

14. Madrid-Wolff J, Boniface A, Loterie D, Delrot P, Moser C. Controlling Light in Scattering Materials for Volumetric Additive Manufacturing. Advanced Science [Internet]. 2022 Aug 1 [cited 2022 Dec 6];9(22):2105144. Available from: https://onlinelibrary-wiley-com.proxy.library.uu.nl/doi/full/10.1002/advs.202105144

15. Bernal PN, Delrot P, Loterie D, Li Y, Malda J, Moser C, et al. Volumetric Bioprinting of Complex Living-Tissue Constructs within Seconds. Advanced Materials. 2019 Oct 1;31(42).

16. Bernal PN, Bouwmeester M, Madrid-Wolff J, Falandt M, Florczak S, Rodriguez NG, et al. Volumetric Bioprinting of Organoids and Optically Tuned Hydrogels to Build Liver-Like Metabolic Biofactories. Advanced Materials [Internet]. 2022 Apr 1 [cited 2023 Jan 31];34(15):2110054. Available from: https://onlinelibrary.wiley.com/doi/full/10.1002/adma.202110054

17. Madrid-Wolff J, Boniface A, Loterie D, Delrot P, Moser C. Light-based Volumetric Additive Manufacturing in Scattering Resins. arXiv physics [Internet]. 2021 [cited 2022 Dec 5]; Available from: http://arxiv.org/abs/2105.14952

18. Futrega K, Palmer JS, Kinney M, Lott WB, Ungrin MD, Zandstra PW, et al. The microwell-mesh: A novel device and protocol for the high throughput manufacturing of cartilage microtissues. Biomaterials. 2015 Sep 1;62:1–12.

19. Gevaert E, Dollé L, Billiet T, Dubruel P, Grunsven L, Van Apeldoorn A, et al. High throughput micro-well generation of hepatocyte micro-aggregates for tissue engineering. PLoS One [Internet]. 2014 Aug 18 [cited 2022 Dec 14];9(8). Available from: https://journals.plos.org/plosone/article?id=10.1371/journal.pone.0105171

20. Hall GN, Chandrakar A, Pastore A, Ioannidis K, Moisley K, Cirstea M, et al. Engineering bone-forming biohybrid sheets through the integration of melt electrowritten membranes and cartilaginous microspheroids. Acta Biomater. 2023 Jul 15;165:111–24.

21. Gonzalez-Fernandez T, Tenorio AJ, Kent Leach J, Kent Leach J. Three-Dimensional Printed Stamps for the Fabrication of Patterned Microwells and High-Throughput Production of Homogeneous Cell Spheroids. 3D Print Addit Manuf [Internet]. 2020 Jun 1 [cited 2023 Jan 12];7(3):139–47. Available from: /pmc/articles/PMC7313638/

22. A Detailed Analysis of the Factors Affecting Printing Accuracy [Internet]. [cited 2023 Nov 7]. Available from: https://www.chitubox.com/en/academy/advanced/a-detailed-analysis-of-the-factors-affecting-printing-accuracy#xy-resolution-and-print-size

23. Model orientation best practices for SLA printing [Internet]. [cited 2023 Aug 9]. Available from: https://support.formlabs.com/s/article/Model-Orientation?language=en_US

24. Guo W, Chen Z, Feng Z, Li H, Zhang M, Zhang H, et al. Fabrication of Concave Microwells and Their Applications in Micro-Tissue Engineering: A Review. Micromachines (Basel) [Internet]. 2022 Sep 1 [cited 2023 Sep 17];13(9). Available from: /pmc/articles/PMC9505614/

25. Thomsen AR, Aldrian C, Bronsert P, Thomann Y, Nanko N, Melin N, et al. A deep conical agarose microwell array for adhesion independent three-dimensional cell culture and dynamic volume measurement. Lab Chip [Internet]. 2017 Dec 19 [cited 2023 Nov 7];18(1):179–89. Available from: https://pubs-rsc-org.proxy.library.uu.nl/en/content/articlehtml/2018/lc/c7lc00832e

26. Selimović Š, Piraino F, Bae H, Rasponi M, Redaelli A, Khademhosseini A. Microfabricated polyester conical microwells for cell culture applications. Lab Chip [Internet]. 2011 Jun 28 [cited 2023 Nov 7];11(14):2325–32. Available from: https://pubs-rsc-org.proxy.library.uu.nl/en/content/articlehtml/2011/lc/c1lc20213h

27. Schmitz N, Laverty S, Kraus VB, Aigner T. Basic methods in histopathology of joint tissues. Osteoarthritis Cartilage. 2010 Oct 1;18(SUPPL. 3):S113–6.

28. Wu Z, Korntner SH, Mullen AM, Zeugolis DI. Collagen type II: From biosynthesis to advanced biomaterials for cartilage engineering. Biomaterials and Biosystems [Internet]. 2021 Dec 1 [cited 2023 Sep 7];4:100030. Available from: /pmc/articles/PMC9934443/

29. De Moor L, Fernandez S, Vercruysse C, Tytgat L, Asadian M, De Geyter N, et al. Hybrid Bioprinting of Chondrogenically Induced Human Mesenchymal Stem Cell Spheroids. Front Bioeng Biotechnol [Internet]. 2020 [cited 2022 Nov 16];8. Available from: www.frontiersin.org

30. De Moor L, Merovci I, Baetens S, Verstraeten J, Kowalska P, Krysko D V., et al. High-throughput fabrication of vascularized spheroids for bioprinting. Biofabrication [Internet]. 2018 Jun 12 [cited 2022 Dec 15];10(3):035009. Available from: https://iopscience.iop.org/article/10.1088/1758-5090/aac7e6

31. Berneel E, Philips C, Declercq H, Cornelissen R. Redifferentiation of high-throughput generated fibrochondrocyte micro-aggregates: Impact of low oxygen tension. Cells Tissues Organs [Internet]. 2016 [cited 2022 Dec 15];202(5–6):369–81. Available from: www.karger.com/cto

32. Futrega K, Robey PG, Klein TJ, Crawford RW, Doran MR. A single day of TGF-β1 exposure activates chondrogenic and hypertrophic differentiation pathways in bone marrow-derived stromal cells. Communications Biology 2021 4:1 [Internet]. 2021 Jan 4 [cited 2023 Aug 11];4(1):1–12. Available from: https://www-nature-com.proxy.library.uu.nl/articles/s42003-020-01520-0

33. Hu DP, Ferro F, Yang F, Taylor AJ, Chang W, Miclau T, et al. Cartilage to bone transformation during fracture healing is coordinated by the invading vasculature and induction of the core pluripotency genes. Development [Internet]. 2017 Jan 1 [cited 2023 Aug 9];144(2):221. Available from: /pmc/articles/PMC5394763/

34. Kanawa M, Igarashi A, Ronald VS, Higashi Y, Kurihara H, Sugiyama M, et al. Age-dependent decrease in the chondrogenic potential of human bone marrow mesenchymal stromal cells expanded with fibroblast growth factor-2. Cytotherapy [Internet]. 2013 [cited 2023 Jul 17];15:1062–72. Available from: http://dx.doi.org/10.1016/j.jcyt.2013.03.015

35. Tacchetti C, Tavella S, Dozin B, Quarto R, Robino G, Cancedda R. Cell condensation in chondrogenic differentiation. Exp Cell Res. 1992 May 1;200(1):26–33.

36. Yu DA, Han J, Kim BS. Stimulation of Chondrogenic Differentiation of Mesenchymal Stem Cells. Int J Stem Cells [Internet]. 2012 [cited 2023 Nov 9];5(1):16. Available from: /pmc/articles/PMC3840987/

37. Horton Jr. WE, Bennion P, Yang L. Cellular, molecular, and matrix changes in cartilage. Musculoskelet Neuronal Interact . 2006;6(4):379–81.

38. Burdis R, Kelly DJ. Biofabrication and bioprinting using cellular aggregates, microtissues and organoids for the engineering of musculoskeletal tissues. Vol. 126, Acta Biomaterialia. Acta Materialia Inc; 2021. p. 1–14.

39. Markway BD, Tan GK, Brooke G, Hudson JE, Cooper-White JJ, Doran MR. Enhanced chondrogenic differentiation of human bone marrow-derived mesenchymal stem cells in low oxygen environment micropellet cultures. Cell Transplant [Internet]. 2010 [cited 2023 Sep 29];19(1):29–42. Available from: www.cognizantcommunication.com

40. Sarem M, Otto O, Tanaka S, Shastri VP. Cell number in mesenchymal stem cell aggregates dictates cell stiffness and chondrogenesis. Stem Cell Res Ther [Internet]. 2019 Jan 10 [cited 2023 Sep 14];10(1):1–18. Available from: https://stemcellres.biomedcentral.com/articles/10.1186/s13287-018-1103-y

41. Lam J, Bellayr IH, Marklein RA, Bauer SR, Puri RK, Sung KE. Functional Profiling of Chondrogenically Induced Multipotent Stromal Cell Aggregates Reveals Transcriptomic and Emergent Morphological Phenotypes Predictive of Differentiation Capacity. 2018 [cited 2023 Sep 12]; Available from: http://dx.doi.org/

42. Foyt DA, Taheem DK, Ferreira SA, Norman MDA, Petzold J, Jell G, et al. Hypoxia impacts human MSC response to substrate stiffness during chondrogenic differentiation. Acta Biomater [Internet]. 2019 Apr 4 [cited 2023 Oct 4];89:73. Available from: /pmc/articles/PMC6481516/

43. Place TL, Domann FE, Case AJ. Limitations of Oxygen Delivery to Cells in Culture: An Underappreciated Problem in Basic and Translational Research. Free Radic Biol Med [Internet]. 2017 Dec 1 [cited 2023 Oct 4];113:311. Available from: /pmc/articles/PMC5699948/

44. Nilsson Hall G, Mendes LF, Gklava C, Geris L, Luyten FP, Papantoniou I. Developmentally Engineered Callus Organoid Bioassemblies Exhibit Predictive In Vivo Long Bone Healing. Advanced Science. 2020 Jan 1;7(2).

45. Murphy KC, Hung BP, Browne-Bourne S, Zhou D, Yeung J, Genetos DC, et al. Measurement of oxygen tension within mesenchymal stem cell spheroids. J R Soc Interface [Internet]. 2017 [cited 2023 Aug 18]; Available from: https://royalsocietypublishing.org/doi/10.1098/rsif.2016.0851

46. Lynch K, Pei M. Age associated communication between cells and matrix: a potential impact on stem cell-based tissue regeneration strategies. Organogenesis [Internet]. 2014 Jul 1 [cited 2023 Aug 10];10(3):289. Available from: /pmc/articles/PMC4594597/

47. Jang J, Park HJ, Kim SW, Kim H, Park JY, Na SJ, et al. 3D printed complex tissue construct using stem cell-laden decellularized extracellular matrix bioinks for cardiac repair. Biomaterials. 2017 Jan 1;112:264–74.

48. Mwale F, Billinghurst C, Wu W, Alini M, Webber C, Reiner A, et al. Selective Assembly and Remodelling of Collagens II and IX Associated With Expression of the Chondrocyte Hypertrophic Phenotype. 2000 [cited 2023 Oct 1]; Available from: https://anatomypubs.onlinelibrary.wiley.com/doi/10.1002/1097-0177

49. Instructions for the mini-beadbeater (typeBX-4) cell disrupter.

50. Gehlen J, Qiu W, Schädli GN, Müller R, Qin XH. Tomographic volumetric bioprinting of heterocellular bone-like tissues in seconds. Acta Biomater. 2023 Jan 15;156:49–60.

51. Chien W, Northrop C, Levine S, Pilch BZ, Peake WT, Rosowski JJ, et al. Anatomy of the Distal Incus in Humans. JARO: Journal of the Association for Research in Otolaryngology [Internet]. 2009 Dec [cited 2023 Oct 28];10(4):485. Available from: /pmc/articles/PMC2774412/

52. Loterie D, Delrot P, Moser C. High-resolution volumetric additive manufacturing HIGH-RESOLUTION VOLUMETRIC ADDITIVE MANUFACTURING A PREPRINT. 2019; Available from: https://www.researchgate.net/publication/334672136

53. Burden D, Gibbons LE, Brangs HCG, Burden DW. Bead Beating: A Primer. 2014 [cited 2023 Oct 28]; Available from: https://www.researchgate.net/publication/293651681

# Appendix

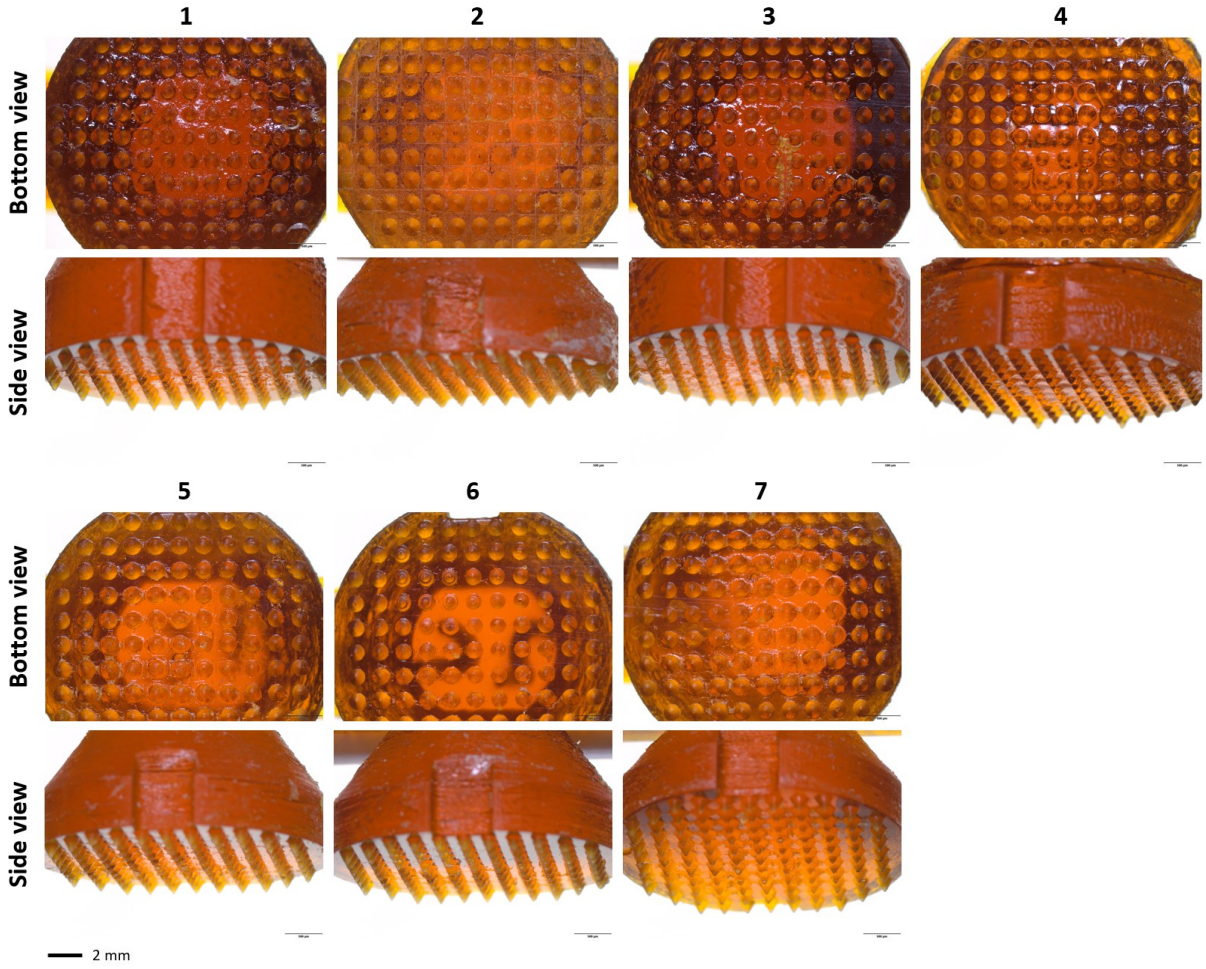


*Appendix 1. Microscopic overview of the DLP printed cone shaped microwell stamps. The microscopic images include a scalebar measuring 2 mm.*

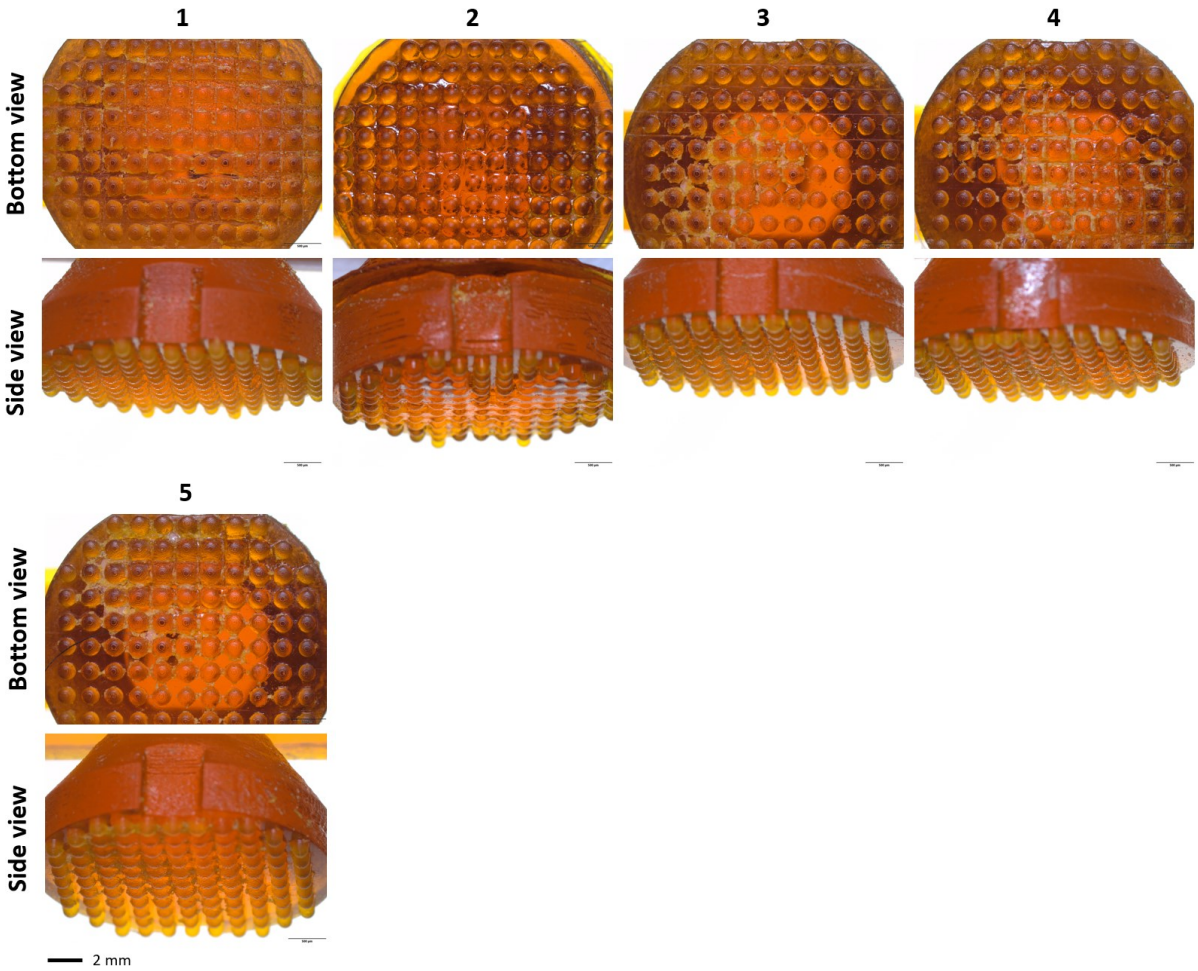


*Appendix 2. Microscopic overview of the DLP printed U-well shaped microwell stamps. The microscopic images include a scalebar measuring 2 mm.*

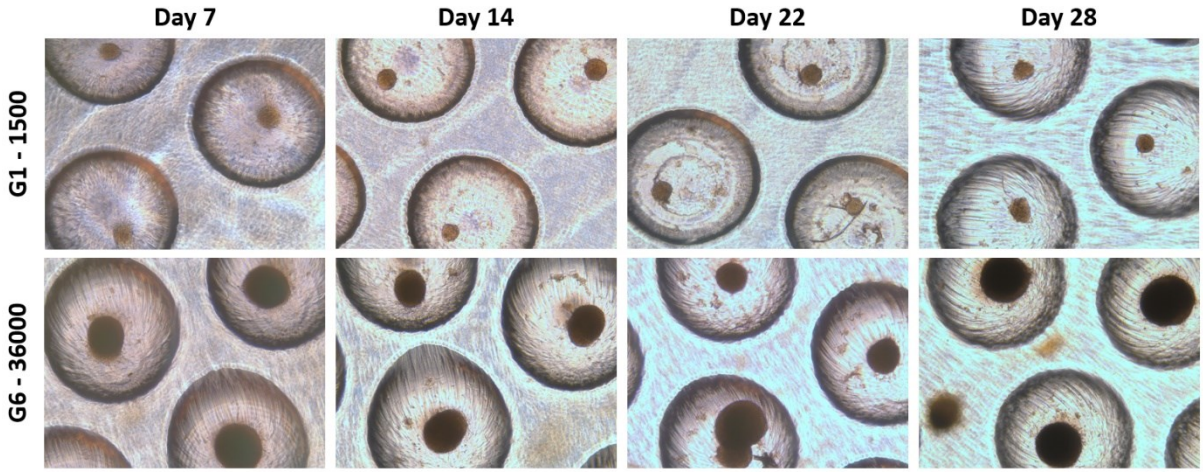


*Appendix 3. Micro pellets of donor C in the microwells during culture on four different timepoints. G1 is group 1 containing 1500 cells per pellet and G6 is group 6 containing 36000 cells per pellet. The images were taken on a Leica DMi1 microscope and white balanced. No scale bar was available.*

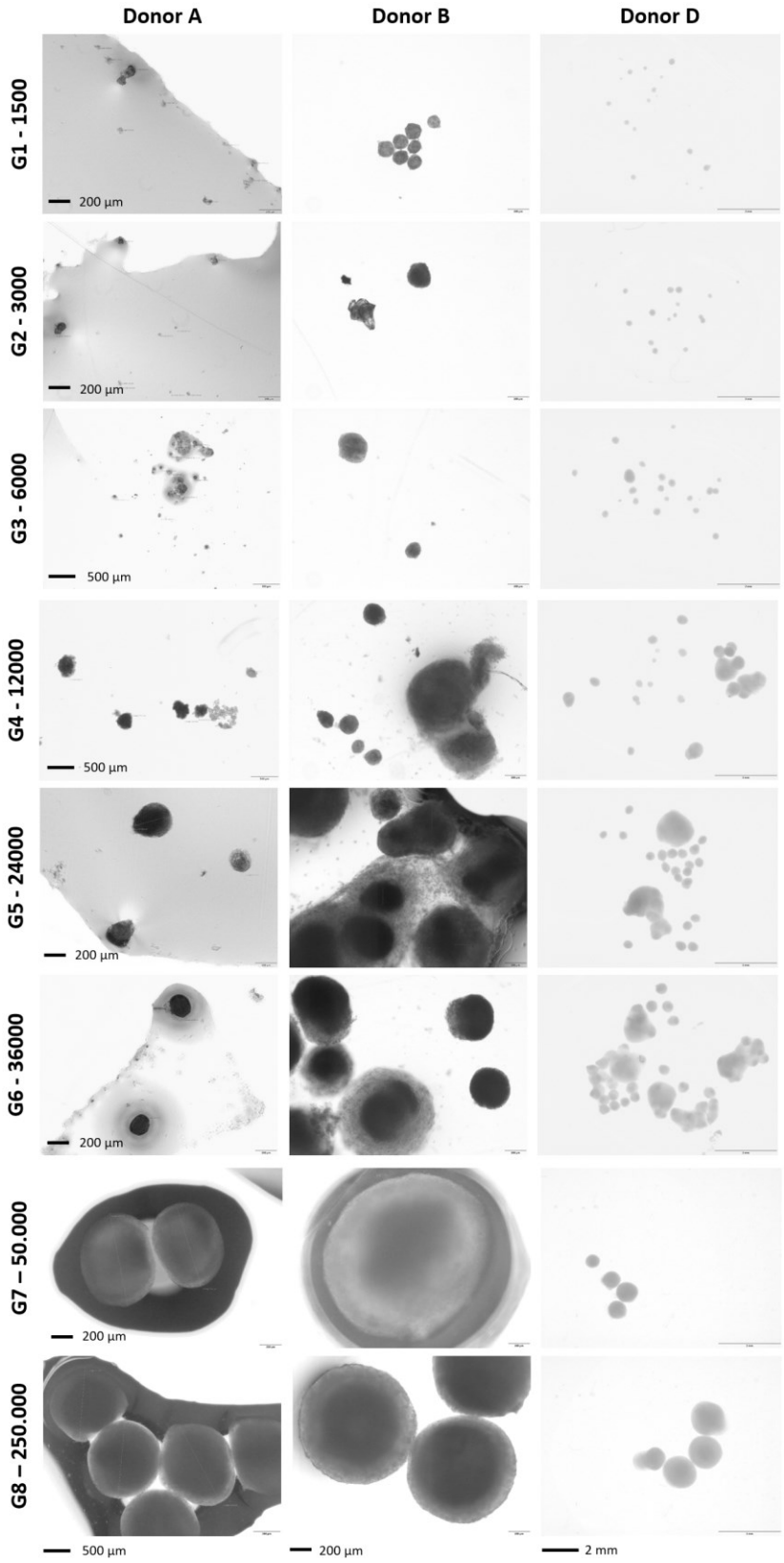


*Appendix 4. Micro pellets and the control from donor A, B, and D in a droplet of 4% formaldehyde. The diameter of the micro pellets was measured in these images. G1-G7 represent the different groups with varying cell densities per pellet: G1 (1500 cells per pellet), G2 (3000 cells per pellet), G3 (6000 cells per pellet), G4 (12000 cells per pellet), G5 (24000 cells per pellet), G6 (36000 cells per pellet), and G7 (50,000 cells per pellet). G8 corresponds to the control group (250,000 cells per pellet. Donor A and B were imaged with the Olympus IX53 microscope and donor D was imaged with the Olympus SZ61 stereomicroscope. The microscopic images include a scalebar measuring either 200 µm or 500 µm for donor A (depending on the group), 200 µm for donor B, and 2 mm for donor D.*

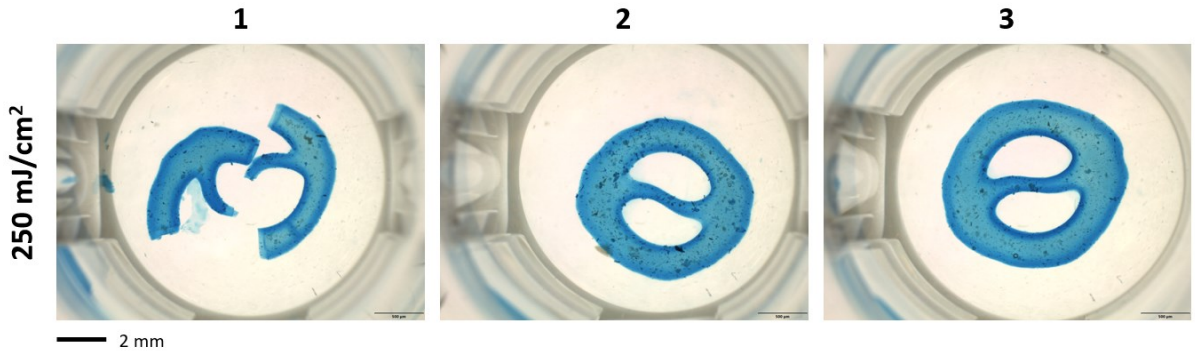


*Appendix 5. Volumetrically printed 'lemon' test shape. A triplicate was printed with a light dose of 250 mJ/cm². The microscopic images include a scalebar measuring 2 mm.*